3-2020

A Method for Routine $PM_{2.5}$ Obsercation and Incorporation into Numerical Weather Prediction

Daniel B. Jagoda

A METHOD FOR ROUTINE $PM_{2.5}$ OBSERVATION AND INCORPORATION INTO NUMERICAL WEATHER PREDICTION

THESIS

Daniel B. Jagoda, 1st Lieutenant, USAF
AFIT-ENP-MS-20-M-102

DEPARTMENT OF THE AIR FORCE
AIR UNIVERSITY

AIR FORCE INSTITUTE OF TECHNOLOGY

Wright-Patterson Air Force Base, Ohio

AFIT-ENP-MS-20-M-102

A METHOD FOR ROUTINE $PM_{2.5}$ OBSERVATION AND INCORPORATION INTO NUMERICAL WEATHER PREDICTION

THESIS

Presented to the Faculty

Department of Engineering Physics

Graduate School of Engineering and Management

Air Force Institute of Technology

Air University

Air Education and Training Command

In Partial Fulfillment of the Requirements for the

Degree of Master of Science in Physical Meteorology

Daniel B. Jagoda, BS

1st Lieutenant, USAF

March 2020

DISTRIBUTION STATEMENT A.
APPROVED FOR PUBLIC RELEASE; DISTRIBUTION UNLIMITED

AFIT-ENP-MS-20-M-102

A METHOD FOR ROUTINE $PM_{2.5}$ OBSERVATION AND INCORPORATION INTO NUMERICAL WEATHER PREDICTION

Daniel B. Jagoda, BS

1st Lieutenant, USAF

Committee Membership:

Dr. Steven Fiorino, Air Force Institute of Technology
Chair

Dr. Steven Peckham, US Army Corps of Engineers,
Engineering Research and Development Center
Member

Dr. Kevin Keefer, Air Force Institute of Technology
Member

Lt Col Robert Tournay, Air Force Institute of Technology
Member

Abstract

Operational numerical weather prediction (NWP) simulates aerosol abundance using climatic emission inventories due to a lack of available real-time observation. An advocation to monitor aerosol number concentration with a standardized global sensor network is defended. A comparison between observations from the existing network "PurpleAir" and condensation particle counters (CPC) reveals the necessity of regulated instrumentation when measuring aerosol number concentration. NWP initialization by the Goddard Chemistry Aerosol Radiation and Transport (GOCART) module is capable of augmentation by hourly aerosol observation. The disparity between observed in-situ particulate matter smaller than 2.5-μm in diameter ($PM_{2.5}$) and Weather Research and Forecasting with Chemistry (WRF-Chem) output—with GOCART—can be reduced via this modification. Analysis is done on WRF-Chem output near Dayton, Ohio after CPC data is manually inserted as WRF-Chem input at the surface. Upon confirmation of $PM_{2.5}$ characterization improvement by point-observation initialization, a method of integrating $PM_{2.5}$ abundance into the long-standing meteorological observation network is suggested: encoding of $PM_{2.5}$ number concentration in the routine meteorological aerodrome report (METAR) as an estimate of horizontal visibility.

This research was completed because of:

My loving wife:	Jeneé Jagoda
My supportive family:	Evan, Denise and Carolyn Jagoda
Additional family:	Jerry and Anita Christensen
Even more family:	The Jagoda, Chance and Buck clans
My brilliant advisor:	Dr. Steve Fiorino
My WRF wizard:	Dr. Steven Peckham
My sensor specialist:	Dr. Kevin Keefer
My steadfast weather leader:	Lt Col Robert Tournay
My accountability crew:	The 20M weather/space-weather class
My morale booster:	Finley (our pet dachshund)

A Haiku:

“how’s that thesis?”

everyone just keeps asking

gallons of coffee

Table of Contents

Abstract iv

Table of Contents vi

List of Figures viii

List of Tables ix

List of Acronyms x

I. Introduction 1

- General Issue 1
- Problem Statement 2
- Hypotheses 3
- Objectives 4
- Preview 5

II. Background and Literature Review 7

- Overview 7
- Atmospheric Composition 7
- Aerosol Measurement Networks 11
- Weather Research and Forecasting with Chemistry (WRF-Chem) 14
- Goddard Chemistry Aerosol and Radiation Transport (GOCART) 16
- Horizontal Visibility 17

III. Methodology 20

- Overview 20
- Generating WRF-Chem Output with GOCART Input 20
- Point-Measurement of $PM_{2.5}$ 23
- Modifying WRF-Chem Input 24
- Encoding $PM_{2.5}$ in METAR 26

IV. Results and Analysis 30

- Overview 30
- WRF-Chem Output with GOCART Input (Unmodified) 30
- Hourly $PM_{2.5}$ Number Concentrations 33
- WRF-Chem Output with Modified Input 35
- Suggestions for Updated METAR 38

V. Conclusions and Recommendations 45

Overview 45
Conclusions of Research 45
Recommendations for Future Study 46
Summary 47

Bibliography 48

List of Figures

Figure 1. Constituent pollutants of $PM_{2.5}$ 8
Figure 2. Sample size distribution of Dayton air with lognormal shape 10
Figure 3. GAW network with archived aerosol data options 12
Figure 4. PurpleAir network in central CONUS 13
Figure 5. WRF-Chem flow of information 15
Figure 6. Snapshot of "unrestricted visibility" prevalence 18
Figure 7. Light extinction and horizontal visibility 19
Figure 8. Domain of WRF-Chem runs 22
Figure 9. PurpleAir sensor and TSI 3788 CPC 23
Figure 10. Sequence of WRF-Chem with input modification 25
Figure 11. LEEDR horizontal visibility construct 28
Figure 12. WRF-Chem vs TAF 31
Figure 13. WRF-Chem $PM_{2.5}$ output over entire domain 32
Figure 14. Meteogram of available parameters 33
Figure 15. Comparison of PurpleAir and CPC 34
Figure 16. Comparison of WRF-Chem $PM_{2.5}$ output pre/post-modification 36
Figure 17. Comparison of WRF-Chem errors pre/post modification 37
Figure 18. LEEDR and transmissometer visibilities 39
Figure 19. Surface pressure and humidity with corresponding visibility 40
Figure 20. Number concentration, humidity, and visibility 41
Figure 21. Number concentration and visibility "best fit" 42
Figure 22. Visibility-Number Concentration conversion error 43

List of Tables and Equations

Table 1. GOCART chemical species and properties 16

Table 2. GADS number concentrations for Dayton, OH 28

Table 3. $PM_{2.5}$ number concentrations and corresponding visibilities 44

Equation 1. Lognormal number-size distribution 9

Equation 2. Aerosol-Related Light Extinction 19

Equation 3. Surface Visibility 19

Equation 4. Mass-Number conversion 24

Equation 5. Number-Visibility conversion 44

Equation 6. Visibility-Number conversion 44

List of Acronyms

AERONET	Aerosol Robotic Network
AFIT	Air Force Institute of Technology
AFRL	Air Force Research Laboratory
AFWA	Air Force Weather Agency
AOD	aerosol optical depth
ARW	Advanced Research WRF
BL	boundary layer
CCN	cloud condensation nuclei
CONUS	Continental United States
CPC	Condensation Particle Counter
EDGAR	Emission Database for Global Atmospheric Research
EPA	Environmental Protection Agency
GAW	Global Atmosphere Watch
GFS	Global Forecasting System
GOCART	Goddard Chemistry Aerosol and Radiation Transport
Gt	Gigaton
HTAP	Hemispheric Transport of Air Pollution
HPC	high performance computing
HTAP	Hemispheric Transport of Atmospheric Pollution
ICAO	International Civil Aviation Organization
IR	infrared
LEEDR	Laser Environmental Effects Definition and Reference
METAR	Meteorological Aerodrome Report
Mm	megameter

µm	micrometer
NCAR	National Center for Atmospheric Research
NEI	National Emissions Inventory
NIR	near-infrared
nm	nanometer
NWP	Numerical Weather Prediction
NWS	National Weather Service
OH	Ohio
OPC	optical particle counter
PM	particulate matter
RETRO	Reanalysis of the Troposphere
RH	relative humidity
SM	statute miles
TAF	terminal aerodrome forecast
TOD	time of day
UV	ultraviolet
VIS	METAR visibility
WMO	World Meteorological Organization
WPAFB	Wright-Patterson Air Force Base
WPS	WRF Preprocessing System
WRF	Weather Research and Forecasting
WRF-Chem	Weather Research and Forecasting with Chemistry

A METHOD FOR ROUTINE $PM_{2.5}$ OBSERVATION AND INCORPORATION INTO NUMERICAL WEATHER PREDICTION

I. Introduction

General Issue

Atmospheric composition is innately linked to various meteorological phenomena. Aerosols that are suspended in the lower troposphere significantly impact local radiative transfer, cloud formation and precipitation, and visibility restriction. Observational methods that quantify the aerosol abundance are utilized by specially-interested parties, but are not commonplace in observational meteorology. Although most of these organizations monitor aerosol mass per volume of air, an essential claim posited in this research is that knowing the *number* of particles smaller than 2.5-micrometers ($PM_{2.5}$) is categorically more descriptive and relevant for weather forecasters and directed energy systems. If a meteorologist fails to characterize atmosphere composition, he or she loses the ability to better predict the aforementioned effects on radiation and condensation. Weather stations around the world maintain equipment that monitor temperature, dewpoint, pressure, and an assortment of other parameters in order to accurately monitor the meteorological state of the atmosphere. This network does not consider atmospheric composition, and lacks the ability to measure ambient aerosol number concentrations. By installing and integrating aerosol measurement sensors at every weather station into routine meteorological aerodrome reports (METAR), our grasp and understanding of the atmosphere could be dramatically enhanced.

Numerical weather prediction (NWP), a foundational technology used in nearly every forecast today, is capable of simulating aerosol emission in most environments. A

leader in this field is the chemically-coupled version of the Weather Research and Forecasting (WRF) model, also known as the WRF-Chem (Grell et al., 2005). While this model has many customizable options to choose when simulating emissions and microphysics, there are no established aerosol networks to provide real-time observations to initialize or verify forecasts. Nearly every meteorological model relies on meteorological observations for initialization; it is logical to suppose that aerosol modeling should also rely on the same, time-relevant observation system. In order to accurately characterize the microphysical interactions of aerosols in our atmosphere, Kahn et al. (2017) suggested a 15-variable observational network to reduce uncertainty predicting "direct aerosol radiative forcing." To demonstrate how simulation of one of these variables—aerosol loading—could be improved with a network of observations, a coordinate corresponding to Dayton, Ohio is manually initialized in multiple WRF-Chem runs over the Central Continental United States (CONUS). The model's forecast is compared to a condensation particle counter (CPC) located near Dayton and improvement is observed after input modification.

Problem Statement

Comparatively, it is easier to accurately simulate synoptic-scale atmospheric dynamics than microscale atmospheric composition over the same domain. Most scientists in the field possess a basic knowledge of these microscale interactions, but NWP and observational meteorology have not yet fully incorporated aerosol measurements into their most-used products. Several research articles and textbooks claim that aerosols—primarily $PM_{2.5}$—have non-negligible impacts on cloud/precipitation formation and light extinction (Liou 2002, Petty 2006, Rogers & Yau,

1996). The principal job of an observational meteorologist is to provide the best available forecast to the customer. If this product does not include at least a basic forcing by aerosol loading, it is ignoring a potential mechanism for weather phenomena of great clientele interest. It should be said that while particle counting sensors are costly and a somewhat newer practice, gravimetric sensors have been easily available for decades. To date, there has not been a successful campaign to integrate real-time aerosol measurement into the well-established meteorological network.

Secondly, the routine reporting system in use today—METAR—loses value when reporting horizontal visibilities greater than 10 statute miles (SM) (or 10 kilometers in countries that use the metric system). Most observations lie in this greater-than-ten range, and all are considered as the same magnitude – unrestricted—even though 10-SM is not equivalent to 10-km. These arbitrary distance thresholds appease the visual needs of pilots on approach for landing, so reports of greater visibility ranges do not particularly intrigue most customers. Aerosols can be present in significant quantities and have meaningful impacts on light extinction in the atmosphere above 10-SM restriction. In addition to visible perception, light extinction interferes with systems that utilize infrared (IR) sensors. This information is completely ignored and lost with the current METAR format.

Hypotheses

Consistent assimilation of surface point measurements will improve the characterization accuracy of $PM_{2.5}$ using NWP. Conditionally, model-forecasted concentrations will likely be improved most in the first 24 hours (Pagowski et al., 2010),

then gradually diminish to pre-modification levels before the end of the +48-hr model run. Since the model only works with $PM_{2.5}$ mass densities, a conversion of CPC data is needed to translate before initialization. Tracking and measuring number concentration will reveal more relevant and useful information to meteorologists than mass density. If a shift in focus within the aerosol measurement community towards obtaining number concentration occurs, more research will reveal obvious links between aerosol abundance and changes to the Earth's radiation budget. These changes are integral in long-term climate modeling and in short-term meteorological forecasts.

Significant measurement discrepancies are expected between sensors that capture different portions of the aerosol size distribution. Differences will be small for mass measurements and greatly exaggerated for number measurements. Disagreement like this would introduce doubts toward the reliability of aerosol monitoring. Device standardization across a network would remove most of these causes for concern. Converting number concentration into a genuine horizontal visibility will seamlessly include ambient $PM_{2.5}$ loading within the existing method of observation with minor adjustments. These adjustments are expected to be unnoticeable to most operators, and serve purely to better inform the meteorologist analyzing the observation.

Objectives

Finding a method that successfully improves WRF-Chem $PM_{2.5}$ characterization is the primary goal. Since this method involves using time-sensitive observations to remain relevant for operational forecasters, a reliable source of real-time data as the basis for this improvement is needed. Then, after a source is decided, experimentation with

different modifications to the model reveals an effective method. If an NWP model that uses climatic emission data is more accurate after ingesting real-time observations, an argument can be set forth to implement a widespread aerosol measurement network (or leverage an existing one) to sustain this improvement.

The secondary objective is to create a convenient technique of reporting aerosol information while ensuring that it remains familiar and recognizable to the entire community. The visibility (VIS) category in the METAR communicates a possible visible range for the average human eye, and the category is reported in units of meters or SM. Instead of relying solely on transmissometers to measure visibility, we propose that the light-extinction properties of aerosols can be encoded as a visibility. The goal is to develop a process of conversion and a final result that is as simple to implement and read as the current VIS category. Doing so would build the case to introduce aerosol measurement to the well-established observational meteorology network.

Preview

Rudimentary examinations of the characteristics/effects of $PM_{2.5}$, capabilities of aerosol monitoring organizations, fundamentals of the WRF-Chem, descriptions of aerosol schemes and emission databases, and regulations of reporting visibility in METAR format are provided. Plans of action for generating unmodified WRF-Chem output, collecting aerosol and other relevant input data, modifying and regenerating new WRF-Chem output, and encoding $PM_{2.5}$ abundances in METAR format are described. The initial WRF-Chem output is tested for meteorological accuracy to ensure reliability. Next, the available number concentration and weather data is organized and prepared for

use. After repeating WRF-Chem runs with new input, the results are tested against the original runs and a CPC. Finally, a sample of number concentration observations are transformed into horizontal visibilities compatible with METAR format.

II. Background and Literature Review

Overview

First, while evidencing the relevancy of aerosols in meteorological processes, we aim to place special emphasis on $PM_{2.5}$. After describing the benefits of monitoring $PM_{2.5}$ for meteorologists and others, the capabilities and methodologies of three established aerosol-monitoring organizations are explored. Then, an appraisal of their candidatures as reliable sources of data for initializing the WRF-Chem. Continuing, a description of the WRF-Chem model, its aerosol schemes, and the climatic emission databases the model uses to forecast aerosol loading are summarized. The final step of laying the foundation for this research was to study the International Civil Aviation Organization's (ICAO) standards of reporting visibility in METAR format. Since aerosols cause the extinction of light, it would be possible to encapsulate aerosol data in the existing VIS category, thereby eliminating the need to add an entirely new category to a decades-old product.

Atmospheric Composition

Aerosols are usually divided into two major categories: coarse and fine (Petty 2006, Liou 2002, Hinds 1999). Coarse particles are typically larger than 2.5-micrometers (µm), particles smaller than 2.5-µm are considered fine, and the smallest of particles (less than 0.1-µm) are referred to as cloud condensation nuclei (CCN), Aitken nuclei, or ultrafine (Petty 2006, Liou 2002, Hinds 1999). Fine and ultrafine particles smaller than 2.5- µm are considered $PM_{2.5}$. While coarse particles impair visibility and human health, they usually only grow to significant quantity during severe events like fires, volcanic eruptions or winds that whip-up earth/debris/sea salt (Rogers & Yau, 1996). This is

because coarse particles are mostly composed of "primary" particles, or those released directly into the atmosphere (EPA, 2015). "Secondary" particles are the results of photochemical reactions involving primary particles like black carbon, sulfur/nitrogen oxides, and ammonia; nearly all secondary particles are considered $PM_{2.5}$ (EPA, 2015). A majority of anthropogenic emissions are considered $PM_{2.5}$ and dominate urban areas, but naturally-occurring $PM_{2.5}$ like smaller dusts/salts are found nearly everywhere (Masiri et al., 2015). In addition to its meteorological relevance (which is discussed later), $PM_{2.5}$ is exceptionally harmful for humans over long exposures because of its size relative to that of the alveoli—the smallest and most important building block of the lungs where oxygen is absorbed into the blood. Coarse particles are deposited in larger hollows of the lungs/airway and are not capable of pervading these crucial regions like fine particles (Xing et al., 2016).

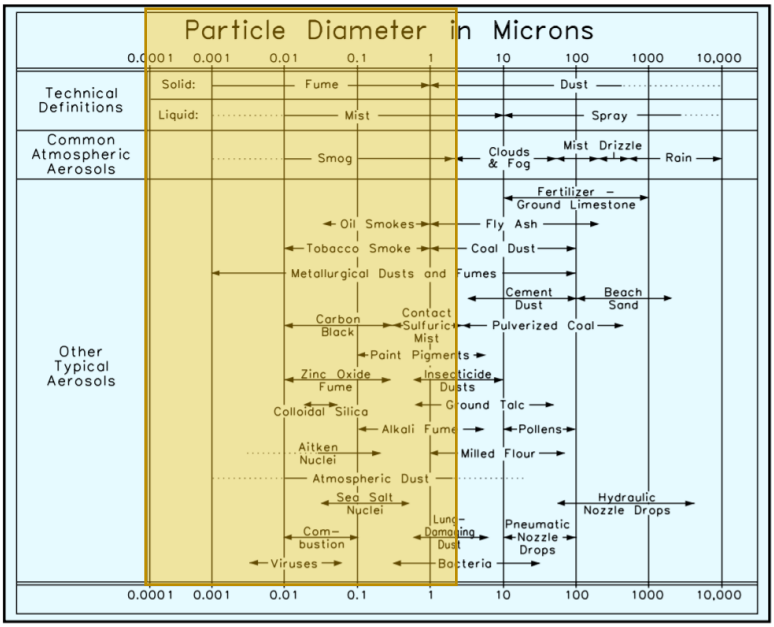

Figure 1. Constituent pollutants that make up $PM_{2.5}$ high-lighted in box (EPA, 2016)

The widely practiced standard for aerosol measurement is mass density, which is normally reported in micrograms per cubic meter (µg m^{-3})(Alfarra, 2004). Number concentration—reported in number per cubic centimeter (cm^{-3})—is used less frequently due to its potential of varied results from different sensors. These disagreements between number concentration measurements arise from instrument sensitivities to particle size detection (Amaral et al., 2015). Sensors normally claim certain "detection efficiencies," or the diameter at which only 50% of particles can be detected. For example, a sensor that can detect particles as small as 10-nanometers (nm) counts hundreds, if not thousands, more particles than a sensor that can only measure down to 500-nm. However, since "a 10-µm diameter particle is equivalent to the mass of one billion 10-nm particles" of the same density, mass measurements don't differ that much among sensors that capture large particles (Alfarra, 2004). For this reason, mass densities favor detection of coarse particles.

Lognormal distributions are commonly found in nature, and can be generally assumed for aerosol size distributions. Peak numbers are found among particle diameters between 10-nm and 100-nm, as seen in Figure 2. The peak of this distribution changes slightly as different amounts and types of aerosols are emitted during the course of the day, but the overall lognormal shape is retained (Amaral et al., 2015). Equation 1 (Koepke et al., 1997) describes number as a function of particle radius (*N(r)*) :

$$\frac{dN(r)}{d(\log r)} = \frac{N_d}{\sqrt{2\pi}\log\sigma} \exp\left[-\frac{(logr - logr_M)^2}{2(log\sigma)^2}\right] \qquad \text{(Equation 1)}$$

where

N_d = *total particle density per unit volume* (normalized to 1)
r = *radius* (m)
r_M = *median radius* (m)
σ = *standard deviation*

Equation 1 can be integrated to calculate the total number concentration. Figure 2 reveals that the majority of a number concentration value is composed by particles less than 100-nm. CCN and other particles smaller than 100-nm are the most susceptible to grow into the accumulation mode due to condensation and coagulation. Homogeneous nucleation, the process of pure condensation without CCN, requires supersaturation of several percent (Rogers & Yau, 1996). However, the presence of CCN increases the likelihood of cloud and eventual precipitation formation even at values of humidity much lower than 100% (Alfarra, 2004; WMO, 2016; Malm, 1999). Constant observation of $PM_{2.5}$ number concentrations would warn meteorologists when these CCN are abundant. Additionally, CCN produce Rayleigh scattering that interferes with near-IR and IR light due to their size relative to the incident light (Petty, 2006).

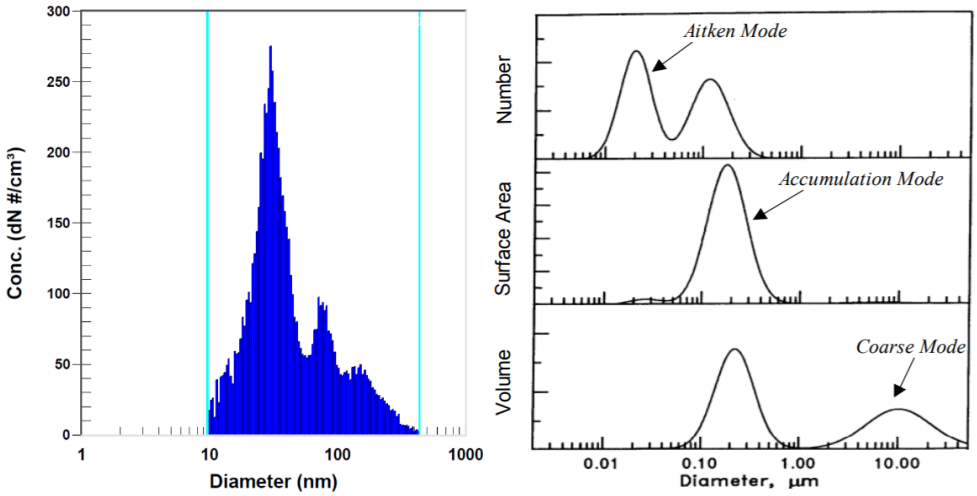

Figure 2. Sample number-size distribution of Dayton air collected by the Center for Directed Energy (Left) that reveals particle abundance in both Aitken and accumulation modes (Right) (Alfarra, 2004)

Aerosol Measurement Networks

While multiple respected organizations are interested in the characterization of atmospheric composition, none of them are recognized as the singular standard source for aerosol data. The United States Environmental Protection Agency (EPA), the Global Atmosphere Watch (GAW), and PurpleAir are three unique parties that maintain equally unique aerosol measurement networks. The EPA holds a diverse number of responsibilities but retains its status as the leading government-led assessor of atmospheric emissions. Every three years the organization releases a National Emissions Inventory (NEI), a detailed report of emission amounts denoted by location, chemical species, and source that includes $PM_{2.5}$ (EPA, 2015). However, emissions are recorded as annual mass amounts (Gt yr^{-1}), and are not suitable for up-to-date model initialization. While the network of sensors the EPA possesses/tracks is extensive, they do not provide real-time $PM_{2.5}$ observations (EPA, 1998). Email inquiry of the EPA in December 2019 regarding a standardized detection efficiency limit for their sensors was a met with a reply from their Ambient Air Monitoring Group. A list of their approved instruments contained only optical particle counters (OPC) instead of CPCs, and they had various efficiencies ranging from 300-nm to 500-nm (EPA, 2016). Since the EPA is most concerned with mass measurements instead of number, detection efficiencies do not affect their results that much, so the decision to employ OPCs rather than CPCs is understandable.

In 1989, the World Meteorological Organization (WMO) created the GAW, a "coordinated global network of observing stations" (GAW, 2020). In 2016, the WMO/GAW published the 2nd Edition of its *Aerosol Measurement Procedures,*

*Guidelines and Recommendation*s (WMO/GAW, 2016). This document is far and away the best foundational material now available for the regulation of a future observational aerosol network. Three of its recommendations for continuous measurement include "particle number concentration (size-integrated), particle number size distribution ... and cloud condensation nuclei number concentration," and the ideal detection efficiency is set as 10-nm (WMO/GAW, 2016). Unfortunately, while the data webpage in Figure 4 showcases the extent of the GAW's network, it does not possess data newer than 1 Jan 2019, and could not be used during this thesis for experimentation with the WRF-Chem. The "Near Real-Time data" hyperlink featured in the bottom left of Figure 3 directs the user to a more limited map of available sensors (none of which are located in the United States) that are recommended for future research.

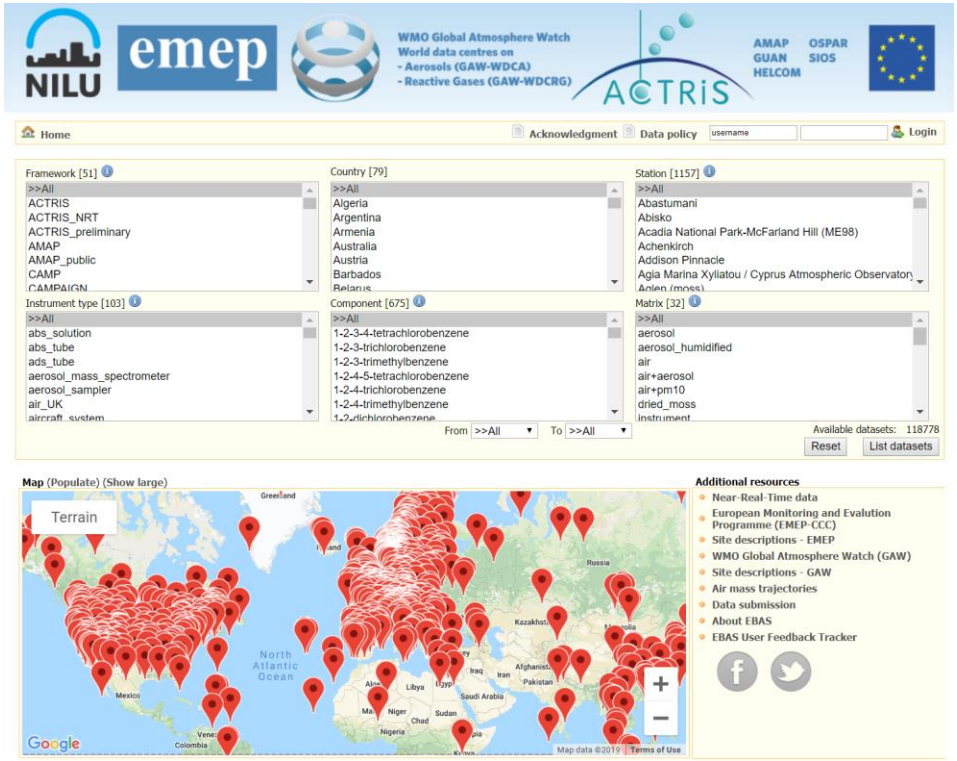

Figure 3. The GAW's archive of data listed by location, instrument, chemical component, and measurement type. (GAW, 2020)

PurpleAir is a limited liability company that markets itself as an "air-quality monitoring solution for home enthusiasts and ... professionals" (PurpleAir, 2020). It is the only organization found during this research that provides real-time $PM_{2.5}$ observations in the domain of interest (central CONUS). Its indoor/outdoor OPCs are available for $259 with internal memory and $229 without, while most CPCs normally cost thousands of dollars. Both PurpleAir OPCs have identical detection efficiencies of 300-nm and provide decent coverage across the globe (PurpleAir, 2020). While this detection efficiency is undesirably high and does not include CCN detection, the network is standardized and states whether a sensor is indoors or outdoors—indicative of its usefulness for meteorologists. Although their mission statement reveals the network's focus on air quality, and their OPCs are unable to measure smaller nanoparticles of interest, PurpleAir's service of providing real-time data to the public is matchless.

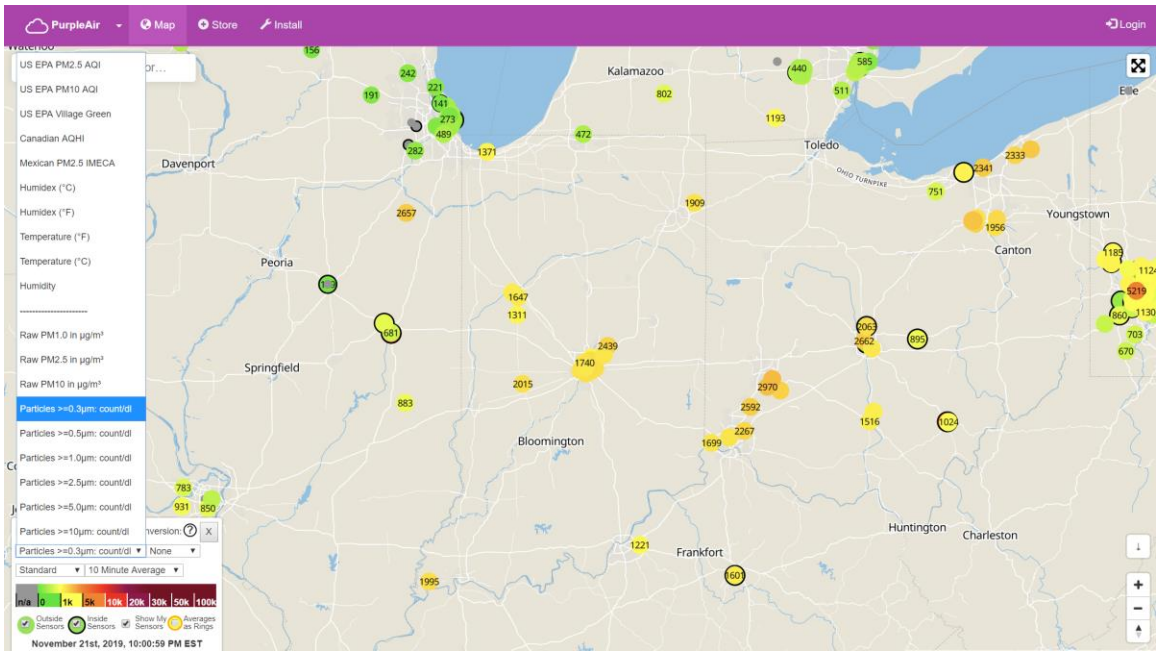

Figure 4. PurpleAir's webpage has a map that can be navigated to regions of interest and view different real-time measurement reports. (PurpleAir, 2020)

Weather Research and Forecasting with Chemistry (WRF-Chem)

NWP was first suggested as a possible forecasting method nearly a century ago, but wasn't a truly worthwhile effort until the advancement of the computer in the 1950's and creation of stable numerical techniques (Lynch 2006, Courant et al. 1928, Klemp & Wilhelmson 1978). The WRF was designed in the 1990's as a collaborative effort between the National Center for Atmospheric Research (NCAR), the Air Force Weather Agency (AFWA), and several other prestigious scientific communities (WRF, 2020). We utilized the Advanced Research WRF (ARW) dynamical solver and its thoroughly-documented webpage dedicated to serving its over 48,000 registered users (WRF, 2020).

Highly customizable and user-friendly, the WRF is now one of the most widely used mesoscale meteorological models in academic research around the world. While the WRF is updateable to Version 4.1 and newer, Version 3.8 was encouraged as a more reliable version for use with the Department of Defense computers used in this study. Both are written in the Fortran and C programming languages. It should be recognized that this advice was quickly accepted from Dr. Peckham—the lead author of the *WRF-Chem Version 3.8.1 User's Guide* (2017) and the coauthor of the WRF-Chem model.

The WRF-Chem is unique due to its coupling within the WRF. The simulated aerosols in the model interact with the simulated radiative transfer from the WRF. The namelist of chemical variable options in the WRF-Chem model is extensive, but the most important one for this thesis is titled "*chem_opt*." Setting *chem_opt* to select integer options greater than zero signifies use of the WRF-Chem rather than the basic WRF. A model run is divided into four principal phases of execution: 1) auxiliary background

input, 2) meteorological pre-processing, 3) chemical pre-processing, and 4) the dynamical core. Anthropogenic, biogenic, and fire emissions are all capable of simulation in the WRF-Chem, but since the city of Dayton is the point of interest in this study, biogenic and fire emissions were not included (since anthropogenic sources are day-to-day the largest contributors to $PM_{2.5}$). Final output can be produced in netCDF format and visualized in Python.

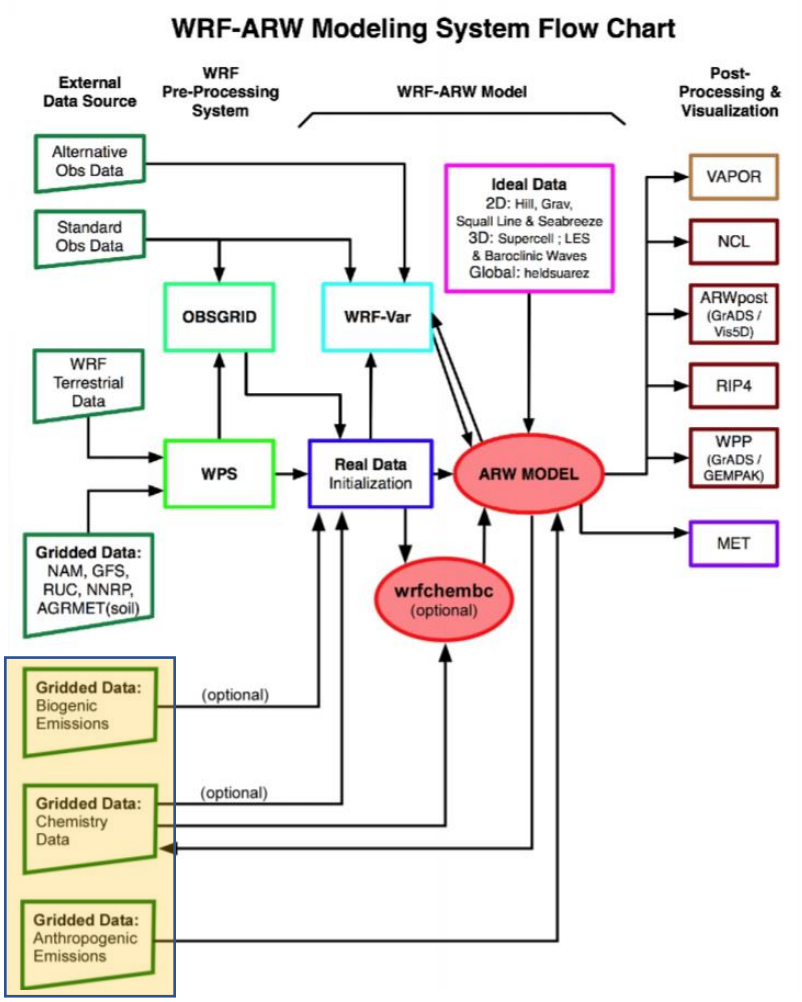

Figure 5. The flow of information in the ARW WRF simulation is identical to that of the WRF-Chem, but the full WRF-Chem includes the gridded elements high-lighted above; this study included only anthropogenic emissions, and visualization with Python was sufficient (Peckham et al., 2017)

Goddard Chemistry Aerosol and Radiation Transport (GOCART)

Aerosol schemes normally fall into three categories: modal, bin and bulk assumption (Kazil, 2009). Modal methods calculate aerosol evolution pertaining to the three mean sizes of the Aitken, accumulation, and coarse modes (Figure 2). Binning methods calculate varying levels of emissions based on specified size ranges/bins. Bulk assumption schemes, like the Goddard Chemistry Aerosol and Radiation Transport (GOCART), only track the masses of individual chemical species, thereby saving time computationally (Chin et al., 2002). This time-per-simulation saved when using GOCART is beneficial for meteorologists that utilize new model data every six hours. The GOCART then assumes an overall lognormal-shape size distribution (described in Equation 1) based on the total mass summation of all chemical species. It calculates a $PM_{2.5}$ variable through summation of sulfates, black carbon, organic carbon, and small dusts/salts, each provided by the emission inventory of choice.

Table 1. GOCART chemical species and physical properties. High-lighted species are included in the $PM_{2.5}$ summation.

Species	Species Abbreviation	Density (g cm^{-3})	Effective Radius (μm)	Real Index Vis/NIR	Imaginary Index Vis/NIR
Sulfate	Sulf	1.80	0.399	1.52	0
Black Carbon (Hydrophobic)	BC1	1.80	0.039	1.85	0.71
Black Carbon (Hydrophilic)	BC2	1.80	0.039	1.85	0.71
Organic Carbon (Hydrophobic)	OC1	1.40	0.087	1.45	0
Organic Carbon (Hydrophilic)	OC2	1.40	0.087	1.45	0
Other PM25	P25	2.65	1.4	1.5	0
Other PM10	P10	2.65	4.5	1.55	0.002
Dust 1	Dust1	2.50	0.73	1.55	0.002
Dust 2	Dust2	2.65	1.4	1.55	0.002
Dust 3	Dust3	2.65	2.4	1.55	0.002
Dust 4	Dust4	2.65	4.5	1.55	0.002
Dust 5	Dust4	2.65	8.0	1.55	0.002
Sea Salt 1	Seas1	2.20	0.3	1.45	0
Sea Salt 2	Seas2	2.20	1.0	1.45	0
Sea Salt 3	Seas3	2.20	3.25	1.45	0
Sea Salt 4	Seas4	2.20	7.50	1.45	0

"Emission Inventories" are datasets of climatic estimates for various chemical species (greenhouse gases, sulfates, nitrates, etc.) developed from years of research and observation. The prescribed amounts of emissions for each species are simulated using GOCART as fluxes at the surface in units of $\mu g\ m^{-2}\ s^{-1}$. Three commonly used inventories include: the EPA's 4-km grid NEI, the 0.5-degree mesh Reanalysis of the Troposphere (RETRO), and the 10-degree Emission Database for Global Atmospheric Research (EDGAR). The temporal resolution of the NEI is hourly, the RETRO and EDGAR are monthly (Peckham et al., 2017). In a 2019 study, all of these databases were tested in the WRF-Chem and significantly underforecasted number concentration values for Dayton, OH (Fiorino et al., 2019). The inventory that performed the best compared to observed $PM_{2.5}$ data in this study turned out to be the Hemispheric Transport of Air Pollution (HTAPv2)(Janssens-Maenhout et al., 2015). The HTAPv2 is regridded for use in the WRF-Chem with spacing of 0.1 by 0.1-degrees, with monthly estimates for several chemical species of interest (PM, black and organic carbon, etc.) that vary by emission sector (source, i.e. transport, industry, residential)(Janssens-Maenhout et al., 2015). While emission inventories in the WRF-Chem model do an overall adequate job of mimicking actual aerosol loading, running the model day-to-day with meteorological climate-data input instead of real analysis likely would not outperform a persistence forecast.

Horizontal Visibility

Horizontal visibility is reported in METAR format according to the Federal Meteorological Handbook No. 1 (FMH-1) in the United States (NOAA, 2017). The METAR is the standard for routine observation practiced by the WMO and ICAO. It is

satisfactory when relating the general meteorological phenomena (i.e. wind, cloud levels, present weather categories) and characterizing physical features (i.e. temperature, pressure, humidity), but falls short when describing atmospheric composition (visibility). At any given moment, it is most likely that a METAR (regardless of location) reads 10 SM or 9999, the thresholds for automated observations (NOAA, 2017). This limit set in FMH-1 conveys an overall dismissal of value for visibilities greater than 10-SM.

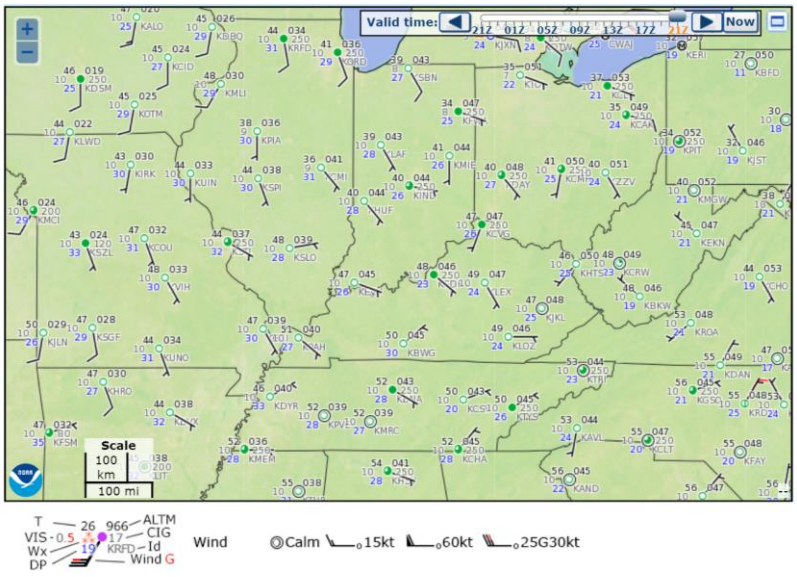

Figure 6. Prevalence of "unrestricted" VIS use (AWS, 2020)

Particulate matter suspended in the air can dramatically impact the extinction of incident light, affecting radiative transfer. This occurs whether the particles are visible as a haze or not. The effects caused by ambient $PM_{2.5}$ are more intense due to their size relative to the visible spectrum, creating a suitable opportunity for both Rayleigh and Mie scattering to occur. Aerosol-related light extinction at a designated wavelength $\beta_{e,s,a}(\lambda)$ can be calculated using Equation 2, and then converted into a horizontal visibility with Equation 3 (Petty, 2006):

$$\beta_{e,s,a}(\lambda) = \int_{r_1}^{r_2} Q_{e,s,a}(n,\lambda,r)\pi r^2 \frac{dN(r)}{rln10*d(logr)} dr \qquad \text{(Equation 2)}$$

Where

$Q_{e,s,a}(n,\lambda,r)$ = aerosol-constituent specific extinction, scattering, absorption

$$Surface\ Vis_{0.55\mu m} = \frac{3.0}{\beta_{e,a}(0)+\beta_{e,m}(0)} = \frac{3.0}{\beta_{e,a}(0)+0.012} \qquad \text{(Equation 3)}$$

Where 3.0 is calculated using the visual contrast at 5% for human perception (0.05) and 0.012-km^{-1} as the average constant of molecular extinction ($\beta_{e,m}$) following Koshmeider's formula (Koshmeider, 1926). *SurfaceVis* is reported in units of km and $\beta_{e,a}$ in inverse kilometers (km^{-1}). It is clear that visibilities much greater than 10-SM or 10-km exist by scattering and absorption. In a clean, aerosol-free atmosphere, the maximum possible visibility (by Equation 3 with molecular extinction remaining) is 250-km.

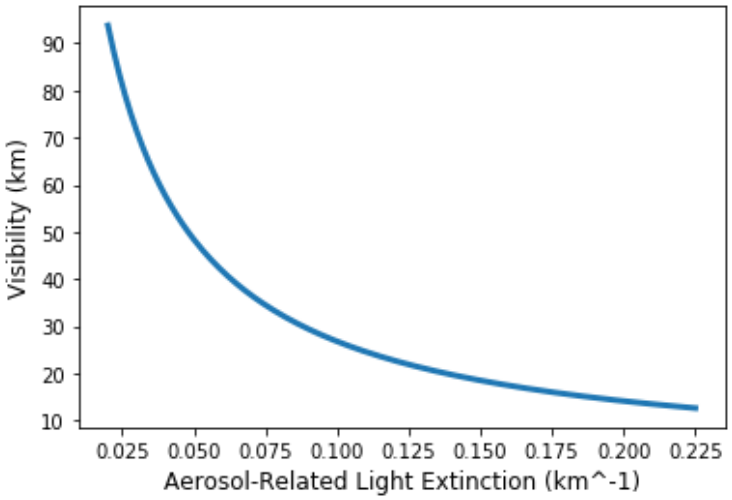

Figure 7. Light extinction and horizontal visibility

III. Methodology

Overview

The ultimate objective of this research is to encourage the integration of $PM_{2.5}$ observation into the existing meteorological observation network. A baseline test is conducted to assess the performance of current aerosol modeling. Next, since initializing the WRF-Chem with real-time aerosol data for Dayton, OH should enhance its accuracy at that point, the capabilities of three different organizations and their respective abilities to provide up-to-date $PM_{2.5}$ data for the model are explored. In doing so, their precisions and reliability for utilization as initialization data in future research efforts are considered. After settling on a benchmark supplier of aerosol data for the WRF-Chem, a method of augmenting the model with new information needed to be designed. Finally, having shown a possible method by which to update an NWP model, a network of aerosol sensors that monitor ambient $PM_{2.5}$ number concentrations must be proposed. These sensors would work alongside the standard instruments already in place at every weather station, working to report METARs to the public. Because aerosols are so closely tied to light extinction, their abundance can serve as a new, more objective basis for measuring horizontal visibility restriction.

Generating WRF-CHEM Output with GOCART Input

We installed a local copy of the WRF-Chem model and its auxiliary data, developed an order of operation in order to run the model, and began producing output. Each simulation/run started at 00Z and produced a forecast of 48-hrs. The first run began 00Z on 1 March 2019 and the last run began 00Z 30 Apr 2019. The numerical mesh for

the simulations used a Lambert-Conformal projection with 134 columns (longitudinal) and 140 rows (latitudinal). Horizontal grid spacing was 0.12-degrees longitudinally and 0.1-degrees latitudinally. The domain of each run (pictured in Figure 8) was centered near Nashville, TN. The northeastern corner is near Toronto, Canada, and the southwestern corner cuts off just north of Houston, TX. The vertical grid (maximum altitude of 10-km) has 12 vertical levels which are vertically stretched to permit higher resolution at the surface in order to capture diurnal variation of the boundary layer and transport of emissions at the surface to the overlying free troposphere. The EDGAR-HTAP emissions inventory was used for all runs (Janssens-Maenhout et al., 2015). EDGAR-HTAP is a version of the HTAPv2 inventory that is augmented by the EDGAR when missing location-specific data.

All WRF-Chem modeling was done on the High-Performance Computer (HPC) "THUNDER." This system resides at the Air Force Research Laboratory (AFRL) on WPAFB, but is scheduled to be decommissioned in March 2020 (AFRL, 2019). This computer was accessible via remote login and could be operated with Linux commands. The scripts used to run the WRF-Chem were submitted in the following order, and are encapsulated in Figure 10: 1) WRF Pre-Processing System (WPS), 2) "Real," 3) Convert, 4) "Real" Part 2, and finally, 5) ARW. Each script was capable of alteration by text editor and ran successively. The WPS script ingests gridded meteorological analysis data every six hours from the Global Forecast System (GFS) as well as static terrain data. The GFS numerical mesh is a 0.25 by 0.25-degree grid with available 00Z, 06Z, 12Z, and 18Z daily analysis from a wide variety of observational data. The first "Real" script submission interpolates this GFS data onto our 0.145 by 0.1-degree WRF grid to form the

initial and lateral boundary conditions, which then merges with the EDGAR-HTAP emission data using "Convert." Full initialization is completed for the WRF-Chem simulation before execution of the ARW script. This process takes between one hour and three hours to complete each run. Some of the notable variable options (and descriptions) chosen for this study include:

chem_opt = 300	(simple GOCART; no ozone since $PM_{2.5}$ is focus)
chemdt = 60	(chemistry timestep in minutes)
kemit = 1	(emissions only at surface; no need for aviation emissions)
emiss_opt = 5	(for use with RETRO/EDGAR)
chem_in_opt = 1	(builds on prior simulation)
bio_emiss_opt = 0	(no biogenic emissions; focus on location in urban area)
dust_opt = 3	(GOCART dust with AFWA; low amounts of dust in Spring)
mp_physics = 6	(WRF Single-Moment 6-Class)
bl_pbl_scheme = 2	(Mellor-Yamada-Janjic scheme)
chem_adv_opt = 2	(monotonic chemical transport)
cu_physics = 1	(Kain-Fritsch scheme)

Figure 8. Simulation domain of the WRF-Chem runs from this thesis; state outlines, boundary coordinates for each corner, and the location of AFIT (Dayton, OH)

Point-Measurement of $PM_{2.5}$

Courtesy of the Center for Directed Energy, this research included a fair amount of hands-on experience with a number of CPCs. In the end, the most recent, accessible data when starting this project was measured by a TSI 3788 water-based CPC. The stream and archive of data from this instrument and other CPCs has grown larger and more consistent over the past year, and is highly recommended for future research. The PurpleAir network allows public download of data from any of its sensors, and a decent number of the ones located in southwestern Ohio had been installed prior to March 2019. Unfortunately, the nearest sensor that shares this longevity is 15 miles away and located in a rural area. WPAFB is not in the immediate vicinity of Dayton, but rather in an urban sprawl slightly east-southeast of the city, so PurpleAir sensors installed in similar locales would be most similar. Seven suitable locations in the suburbs of Columbus, OH, Cincinnati, OH, and Indianapolis, IN were identified (PurpleAir, 2020).

Figure 9. A PurpleAir sensor can be discreetly installed (PurpleAir, 2020) (Left), the TSI 3788 is capable of 2.5-nm particle detection (TSI, 2018) (Right)

Since PurpleAir currently sells instruments with a detection efficiency of 300-nm, the number concentrations they report are much lower than that of our CPC, which counts particles as small as 2.5-nm. To account for this disparity and simulate a more reasonable comparison between the two sensors, the mass densities reported by a PurpleAir sensor in northwestern Columbus were converted to number concentration estimates using Equation 4 (similar to that of Fiorino et al. 2019, but using a median size assumption rather than integrating over the lognormal distribution shown in Equation 1):

$$N = \frac{M}{\rho_M * \frac{4}{3}\pi r_M^3} \qquad \text{(Equation 4)}$$

Where

N = *number concentration* (cm^{-3})
M = *mass density* ($\mu g\ m^{-3}$)
ρ_M = *median density* ($g\ cm^{-3}$)
r_M = *median radius* (μm)

Because the ultrafine particles smaller than PurpleAir's detection limit don't possess substantial mass, the mass densities from their sensors should be convertible to number concentrations within reasonable error of our CPC.

Modifying WRF-CHEM Input

In order to start each WRF-Chem run at 00Z with the right amount of $PM_{2.5}$, a list of the 00Z observations from our CPC needed to be collected. These observation values were manually inserted into the "wrf_chem_input" file to initialize each 24-hr run, and HTAP-produced values at all other locations and heights remain unmodified. The 00Z input file is not produced until after gridded background, meteorological, HTAP and GOCART data have been initialized and formatted for use in the ARW. In order to access and alter it before being run in the ARW script, the WRF-Chem scripts were edited to

pause after “Real” Part 2. The netCDF wrf_chem_input file was then converted to an indexed text file and downloaded. Then, locating the specific surface location-coordinate value in the indexed arrays and changing it to the CPC observation value (which was converted to mass density with Equation 4) would initialize the point for Dayton, OH. Emission rates governed by HTAP remain unmodified at the Dayton coordinate for the duration of the +48-hr simulation; the only change made in this step is the initial (00Z) $PM_{2.5}$ value at the surface. After conversion back to netCDF format and replacement of the original wrf_chem_input, the final script (ARW) of the model was initiated.

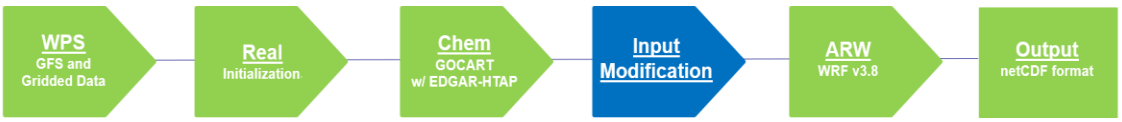

Figure 10. Input is modified right before the ARW core is run

After all modified runs were completed, changes to the original WRF-Chem’s meteorology (i.e. temperature, precipitation, winds) were monitored to see if the new $PM_{2.5}$ concentrations impacted the weather characterization. The hypothesis that the effects of adjusted initialization would mainly disappear within the first 24 hours of each run were also tested. This would be proven if the model returned to original predicted levels near the +24-hr mark. $PM_{2.5}$ output was then converted to number concentration with Equation 4 and compared to the CPC observations in both amount and trend. Other methods than the one developed here for WRF-Chem initialization exist, and could be used to alter emissions or aerosols throughout the entire column of air rather than only ambient $PM_{2.5}$ levels at the surface (Werner et al., 2019). If so, CPC observation down to at least 10-nm or converted PurpleAir data are recommended for use as input.

Encoding $PM_{2.5}$ in METAR

One monumental introduction to observational meteorology would be to include the aerosol-based visibility range in METAR format. The magnitude of these visibilities would, most often-times, remain non-integral to the daily operations of the pilots dependent on these values. This is because more often than not, observations at stations carry the tagline of an "unrestricted" 10 SM or 9999 (shown in Figure 6), each of which are used to mean the same thing despite being two different distances. These values are defined as the thresholds for automated observations in the FMH-1. Any visibility greater than 10-SM or 10-km is reported as 10 SM or 9999 for convenience since no perceived value is attributed to these measurements. While not pertinent to pilots during takeoff/landing, the detection of minor visibility restrictions greater than these thresholds (caused by aerosol light extinction) can be very helpful for meteorologists or directed energy research to indicate varying amounts of aerosol loading.

Simply considering ways to change the most commonly-used product in observational meteorology is daunting. The METAR has remained largely unchanged for more than 50 years, so it is more advantageous to propose an update that fits the existing framework (rather than add something entirely new). The ultimate aim is to include $PM_{2.5}$ number concentration with the rest of the parameters that the meteorological field has deemed important enough to routinely report at least once an hour. This can be done by exploiting the innate tie to light extinction that $PM_{2.5}$ possesses. Through the use of the Laser Environment Effects Definition and Reference (LEEDR) code, it is possible to calculate the amount of light extinction associated with several aerosol number concentration observations, then manually convert these extinctions into horizontal

visibilities using Equation 3 (Center for Directed Energy, 2018). The reverse of this process is also possible: back out an extinction from a horizontal visibility, and from that value, estimate a corresponding number concentration. An example of this two-step process is presented in the results of this thesis, but other plausible conversion methods are left for future research.

LEEDR calculates light extinction using four primary input parameters: number concentration, temperature, dewpoint temperature, and surface pressure. It is important to note that those last three input parameters are already routinely measured for use in the METAR. The data used in this thesis for the months of March and April 2019, as well as a construct to calculate total aerosol and molecular light extinction (previewed in Figure 11) was provided by committee member Dr. Kevin Keefer and sourced by the Center for Directed Energy. He also marked sections of LEEDR code that could be manually adjusted to define the aerosol haze's complex index of refraction, size distribution, and incident wavelength of light. In agreement with NOAA (2019) practices, the entire bulk aerosol is assumed/approximated to have complex refractive index $n = 1.530 - 0.010i$, the same as ammonium sulfate. LEEDR uses this n in the Mie calculations of Equation 2. Lastly, 550-nm was chosen as the appropriate wavelength to monitor for extinction in the visible spectrum (WMO, 2008).

The LEEDR code also assumes a lognormal size distribution of particles in the haze. For this research, the entire bulk aerosol was assumed to be composed of water-soluble aerosols. In order to take chemical species, particle shape and abundance into account, LEEDR has latitude, longitude, and time inputs to use location-specific and

season-specific climate data from the Global Aerosol Data Set (GADS)(Koepke et al., 1997). The number concentration input parameter is scaled to the GADS total during processing, which is shown in Figure 11.

```
function outStruct = calcScaledSurfaceAerosols_DP_abs_sca_aerotype_data(wls, lat, lon, season, tod, sfcAeroConc, sfcTemp, sfcPress, sfcDP, maxAlt)
    % wls [double]: A single wavlength or vector of wavelengths to compute
    %               aerosol effects for.
    % lat [double]: Latitude to compute profile at.
    % lon [double]: Longitude to compute profile at.
    % season [string]: 'Summer' or 'Winter', used to toggle GADS database
    %                  references
    % tod [string]: ExPERT local Time Of Day. Should mimic options from the
    %               list available in the GUI.
    % sfcAeroConc [double]: total measured surface concentration of
    %                       aerosols
    % sfcTemp [double]: Measured Surface Temperature (F)
    % sfcRH [double]: Measured Surface Relative Humidity (%)
    % sfcPress [double]: Measures surface pressure (mb)
    % maxAlt [double]: The maximum altitude (m) to cut off the plots.

    % Example1: calcScaledSurfaceAerosols(4e-6, 39.75, -84.19, 'Summer', '12-15', 347, [], [], [], 1000);
    % Example2: calcScaledSurfaceAerosols(linspace(1e-6, 10e-6, 10), 39.75, -84.19, 'Winter', '03-06', 1215, [], [], [], 1000);
```

```
% Aerosols
numberDensitiesMatrix = Aerosols.calcGADSAerosol(lprof);
nds = sum(numberDensitiesMatrix,2);
lprof.inputs.setAerosolScalar(sfcAeroConc(i)/nds(1));

numberDensitiesMatrix(1, 1) = 0; % parts/cm^3
  numberDensitiesMatrix(1, 3) = 10;
numberDensitiesMatrix(1, 8) = 0;
numberDensitiesMatrix(1, 10) = 26000.5;
```

Figure 11. Total aerosol and molecular extinction in LEEDR with adjustable GADS distribution boxed in red (Center for Directed Energy, 2018; Koepke et al., 1997)

By assuming a constant refractive index, a specific incident wavelength, and a 100% water-soluble composition for GADS (example in Table 2), calculating light extinction can be standardized across locations. Otherwise, since the amounts of individual chemical species present in the atmosphere fluctuates constantly (across locations and time), in-situ measurements of each species would need to be taken constantly to assign optical properties to a haze when performing this calculation. Because of these assumptions, the conversion function derived in this thesis that links $PM_{2.5}$ number concentration to horizontal visibility can be used at any location around the world.

Table 2. GADS number concentrations for Dayton, Ohio (Koepke et al., 1997).

SEASON	INSOLUBLE (cm^{-3})	SOOT (cm^{-3})	WATER-SOLUBLE (cm^{-3})	TOTAL NUMBER CONCENTRATION (cm^{-3})
Default Winter	0.5	15,000	11,000	26,000.5
Default Summer	0.5	15,000	13,200	28,000.5
Custom	0.0	0	26,000.5	26,000.5

Converted visibility estimates can be measured and reported using a CPC instead of a transmissometer. The particle counter would not replace the transmissometer entirely, but rather augment the instrument when visibility restrictions are due solely to aerosol effects. Hydrometeor (fog, rain, snow, etc.), dust, smoke, and volcanic events produce visibility restrictions that far outweigh those of ambient aerosol concentrations. During these events, manual observation and transmissometers should still be utilized, and the METAR should show a present weather remark next to the prevailing visibility. The analyzing meteorologist would recognize that a $PM_{2.5}$ number concentration cannot be obtained from this visibility observation.

When present weather is not occurring, the VIS category would read slightly different than usual. In metric format, where the VIS is reported in meters as four digits (VVVV), the first digit is always a "9" if a CPC is reporting the visibility estimate. This serves to benefit non-meteorological customers that, while reading, immediately notice with the first digit that they do not need to be concerned with restricted visibility. From their perspective, this first "9" functions exactly the same as a 9999 reading. For interpreting meteorologists though, the focus becomes shifted to the last three digits (9VVV). Instead of meters of visibility, the remaining digits of a 9VVV report are in hundreds of meters. For example, if a particular number concentration is converted into a 15.5-km visibility, the category would read "9155," a 20-km visibility is "9200," and 27.5-km is "9275." Converted visibilities are always rounded to the nearest half-kilometer, so the middle two digits represent visibility in kilometers, and the last digit of the category is always be a 0 or 5 to represent whole or plus one-half kilometers. METARs that use imperial units report as normal—in whole SM.

IV. Results and Analysis

Overview

The numerous examinations of WRF-Chem simulations, aerosol data, and converted visibility estimate data in this research produced overall satisfying results. Prior to modification, the WRF-Chem output was subjected to meteorological-accuracy tests and proved relevant and dependable for emission forecasts. It performed well within an acceptable range of actual observations. $PM_{2.5}$ measurements from both a CPC and a PurpleAir sensor were shown as interchangeable, proving PurpleAir as a possible source of data for future model initialization. The CPC number concentrations that were used to initialize new WRF-Chem runs improved the model's $PM_{2.5}$ characterization. The same CPC data was used as input for LEEDR and was successfully converted to horizontal visibilities capable of usage in METAR format. Introducing routine aerosol measurement into observational meteorology in this fashion should encourage future enhancement of NWP and provide standardized sources of data for directed energy research.

WRF-Chem Output with GOCART Input (Unmodified)

After producing WRF-CHEM output for the months of March and April 2019, the weather results were tested for accuracy. If the model were proven wildly inaccurate meteorologically, the reliability of the emission output would be dubious at best. This turned out not to be the case. Temperature, wind speed, and wind direction were compared to observations taken at eight civilian and military airfields: 1) Dayton (KDAY), 2) WPAFB (KFFO), 3) Detroit (KDTW), 4) Selfridge (KMTC), 5) Fort Knox

(KFTK), 6) Louisville (KSDF), 7) Omaha (KOMA), and 8) Offutt (KOFF). The WRF-Chem consistently performed better than the manually-written terminal aerodrome forecast (TAF) at these locations, and the difference (*observation – forecast value*) is visible in Figure 12.

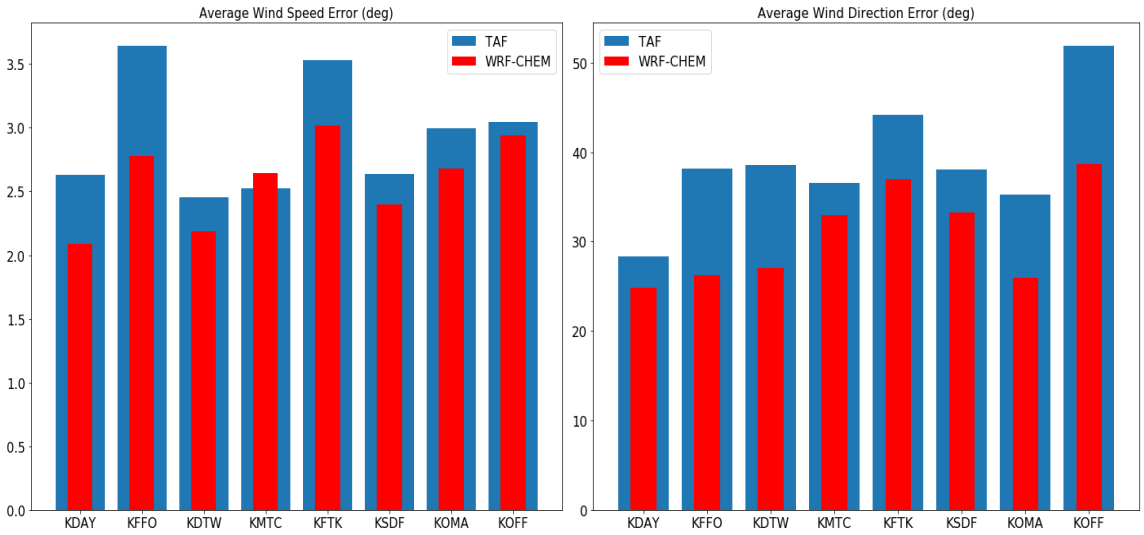

Figure 12. The WRF-Chem's hourly wind speed error compared to TAF error (Left), WRF-Chem outperformed at all locations for wind direction (Right)

With regard to aerosols, the model produced realistic diurnal fluctuations of $PM_{2.5}$ mass with varying amounts of hourly aerosol abundance. All quantities were represented in units of mass over the domain (pictured in Figure 13) with similar magnitudes to those of real observations (between 0-µg m^{-3} and 500-µg m^{-3}). Peak $PM_{2.5}$ levels normally occurred overnight, between 01Z and 11Z (9pm – 7am local time for Ohio). While this coincides with observable trends of aerosol mass in urban areas, it is not the same for trend for particle number (Backman et al., 2012). Number concentrations are at their highest during the afternoon, when peak solar activity maximizes the rate of secondary particle formation and anthropogenic emissions are still strong, and near sunset, when the

boundary layer lowers. This diurnal cycle is discernible in Figure 16 where WRF-Chem simulation values peak earlier than the CPC.

Because the model only calculates $PM_{2.5}$ mass and not the total number, its output needed to be converted using Equation 4 to compare to that of a CPC. Experimentation with different values of r_M for different times of day (since size distributions naturally undergo diurnal variation) proved that setting r_M=0.075 during daytime hours (12Z-00Z in Ohio) and r_M=0.09 at night produced the closest fit between the two sensors. This assumption worked well for Spring but may not necessarily represent the size distribution during other seasons. Judging from GOCART chemical speciation in Table 1 and proven during error-testing, ρ_M=1.8 fit best. These values and times were also used to convert data from the modified WRF-Chem output and PurpleAir mass measurements.

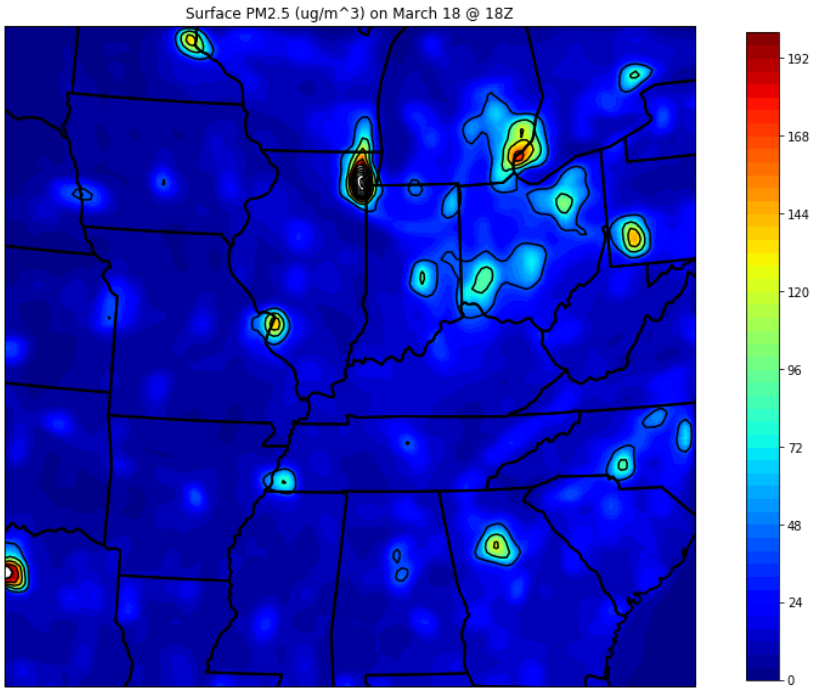

Figure 13. A plot of surface $PM_{2.5}$ mass densities from the WRF-Chem simulations using HTAP emissions reveals anthropogenic sources (mainly urban centers)

Hourly $PM_{2.5}$ Number Concentrations

Along with the CPC located on-site at WPAFB, a litany of other atmospheric parametric data (plotted in Figure 14) was collected by a co-located sensor array. These parameters were paired with the observed number concentration to attempt identification of meteorologically-based trends. While nearly 100% of observations that consisted of high temperature, high RH, high winds, and low pressure were associated with number concentrations between 2000-cm^{-3} and 9000-cm^{-3}, no other major connections were found in the data from March and April 2019. If additional weather/aerosol relationships could be identified from larger sample sizes, observation trends could be leveraged when forecasting $PM_{2.5}$.

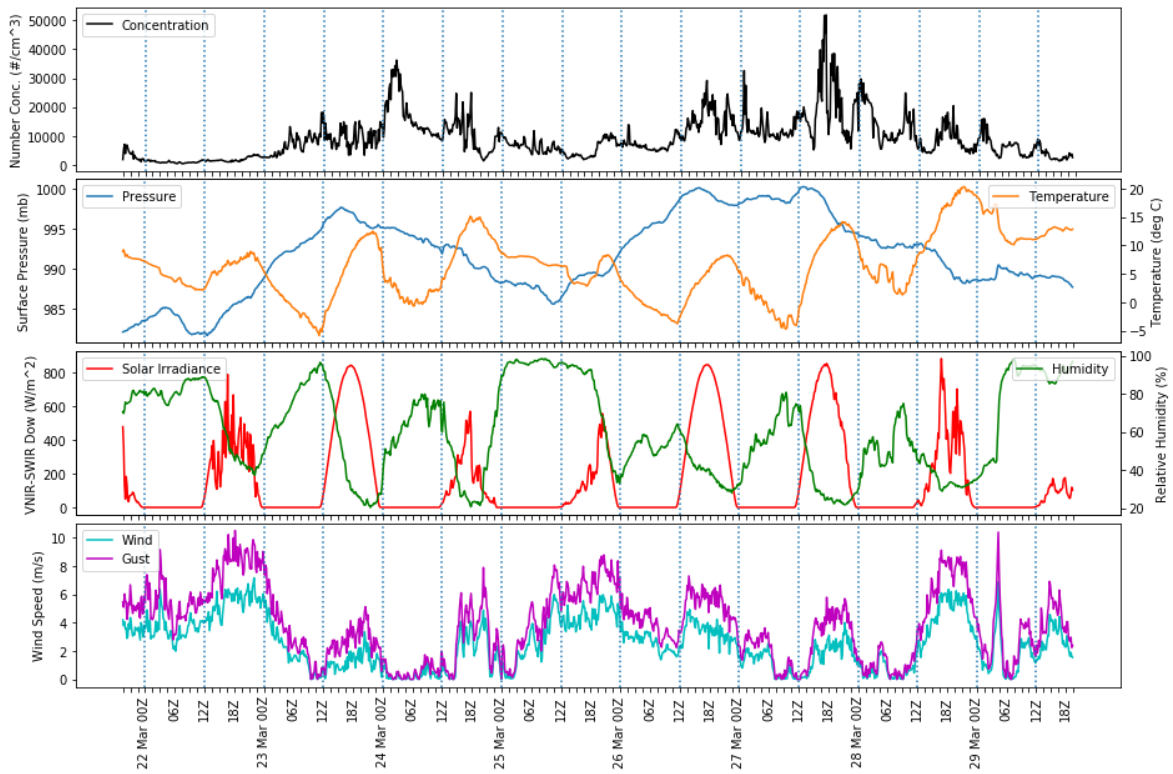

Figure 14. Atmospheric parameters available for comparison

The observed $PM_{2.5}$ number concentration trends of sensors partially downwind of major cities in the Ohio River Basin were examined, and found each of their trends resembled the CPC at AFIT well. Comparisons were done after converting from mass density to number concentration with Equation 4 and the median radius/density values set in the previous section. Because the Purple Air sensor represented in Figure 15 is in northwestern Columbus, OH, it was not expected to reveal identical amounts of $PM_{2.5}$. More importantly, the two sensors revealed similar timing of the aerosol diurnal cycle. Peak emissions were identified in both sets most often near solar noon (00Z) and sunset (18Z). For this reason, PurpleAir shows potential to serve as a source of real-time aerosol data for WRF-Chem initialization in the future. In addition, its mass measurements can be ingested directly without conversion since the model also operates in units of $\mu g\ m^{-3}$.

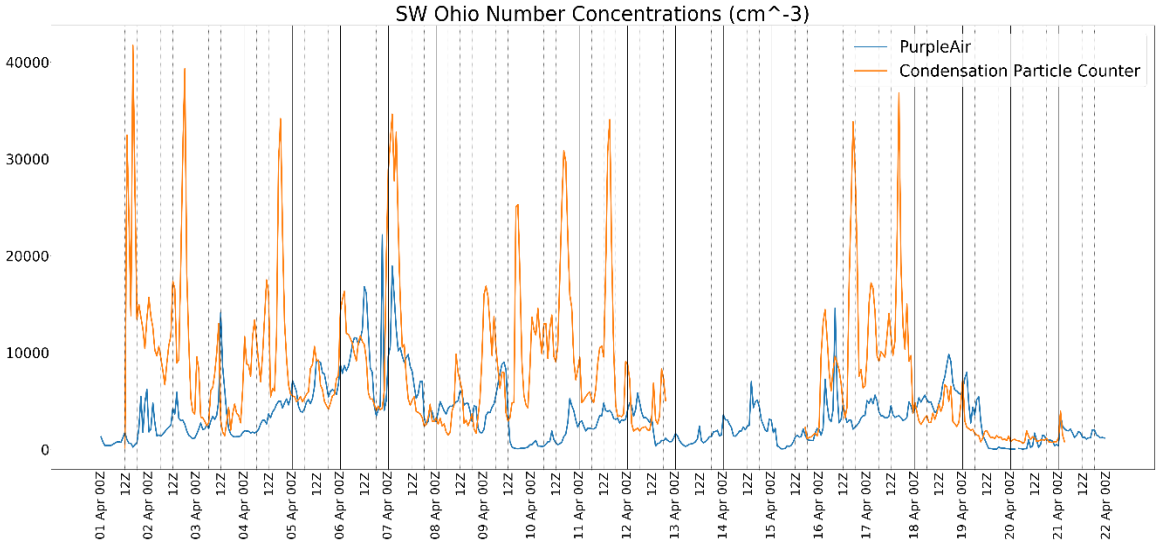

Figure 15. A comparison of converted PurpleAir number concentration values in Columbus, OH and a CPC at WPAFB

WRF-Chem Output with Modified Input

There were no observable changes to the meteorology of the WRF-Chem after modification. Meteorology in the WRF-Chem may be affected if different/multiple points are modified, or if the model is run over longer periods of time. Even though the model doesn't incorporate number concentrations into its calculations for cloud/precipitation formation or temperature, it doesn't mean that the $PM_{2.5}$ values produced by the model cannot be manually interpreted by forecasters and taken into account during analysis. Additionally, climate studies that incorporate the cumulative effects of aerosols on the radiative balance over long periods of time would benefit from knowing the abundances of those aerosols.

Hourly number concentrations of the modified WRF-Chem simulations and the CPC are shown in Figure 16. It should be noted that error comparisons are made after pre-processing WRF-Chem mass densities to resemble number concentration using Equation 4 with the same median time-of-day radius/density used for PurpleAir values. This pre-processing provides a handicap for the model's true forecast performance. After placing each hourly number concentration error into a bin of particular magnitude, the frequencies of occurrence for each bin were recorded in the form of a histogram. Figure 17 shows "amount errors" in terms of cm^{-3} where *amount error = forecast – actual* . More often than not, the WRF-Chem simulation underforecasted number concentrations. The average amount error (absolute value) was 6222 cm^{-3} prior to modification, and was slightly increased to 6245 cm^{-3} afterwards. However, the number of severe underforecasts (more than -20000 cm^{-3} difference) was reduced by 17%, and the number of smallest errors (within 1500 cm^{-3} from true) was increased by 9%.

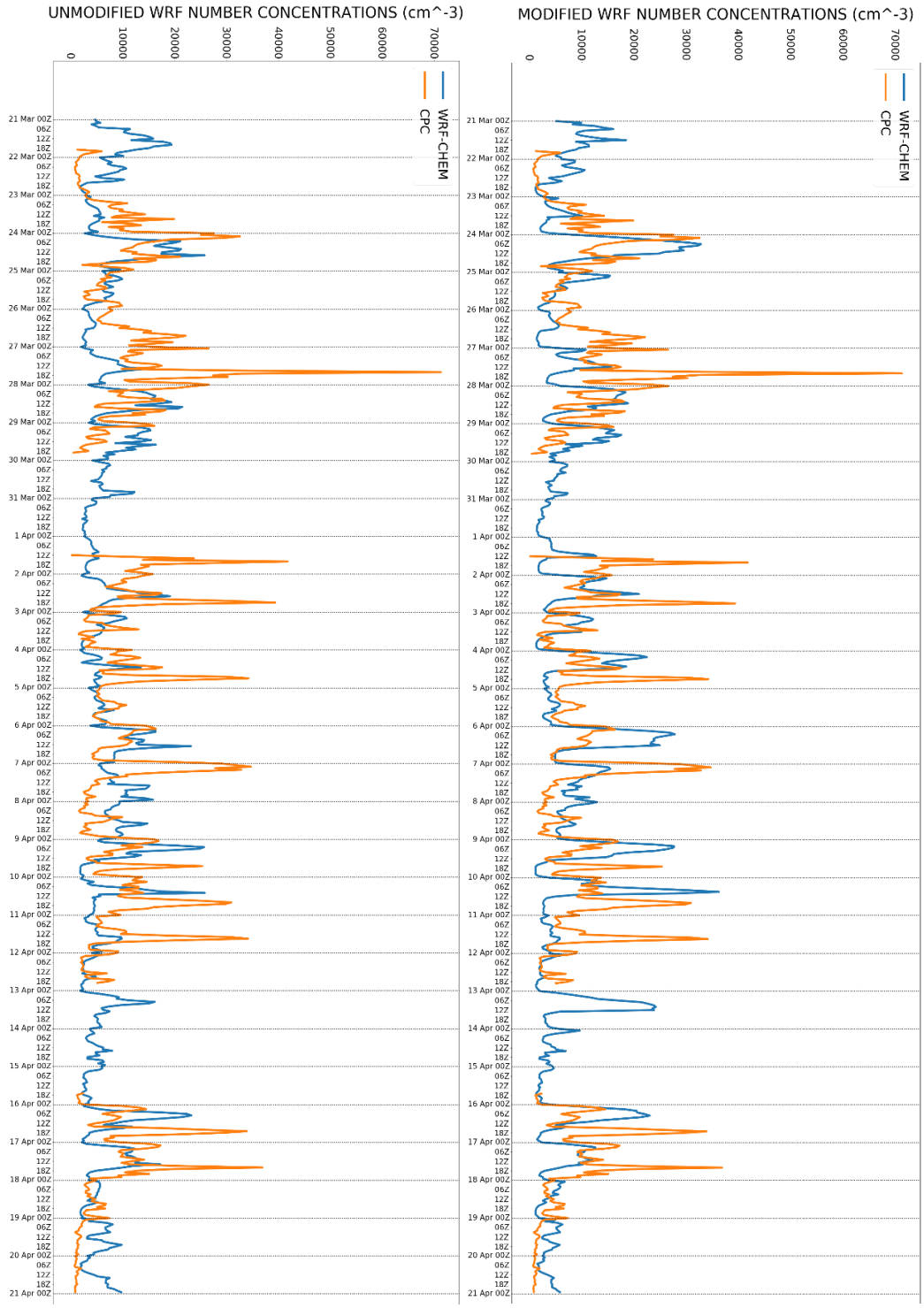

Figure 16. A Comparison of WRF-Chem $PM_{2.5}$ output pre/post modification; each vertical line delineates a new 48-hr WRF-Chem simulation (only the first 24-hrs from each run are plotted)

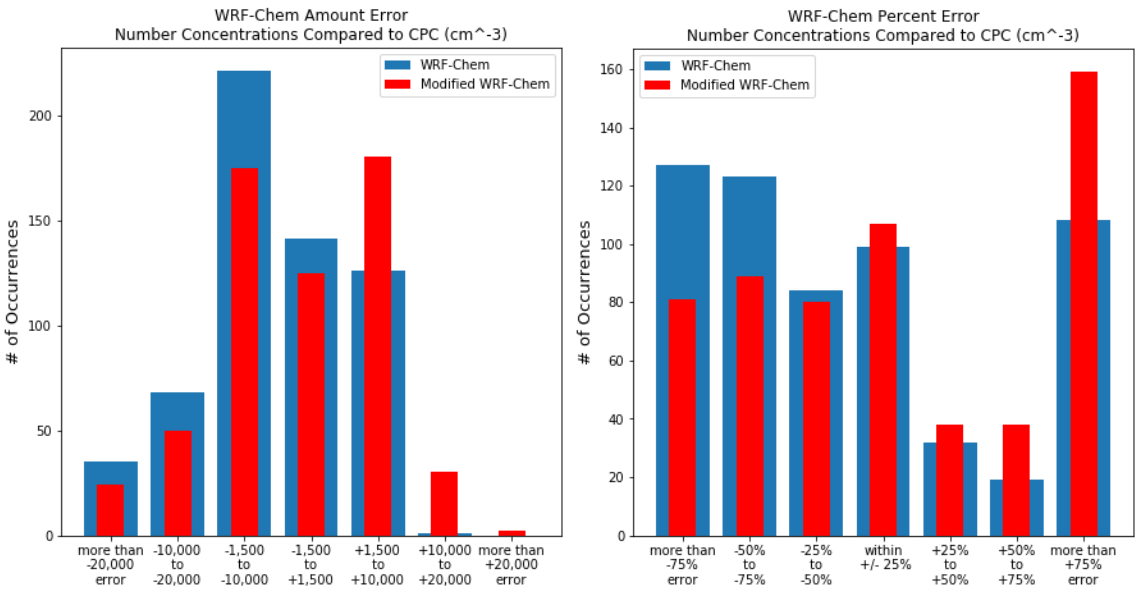

Figure 17. Comparison of WRF-Chem $PM_{2.5}$ characterization pre/post modification.

Amount errors are generally useful when making quick judgements about the accuracy of a system, but don't reveal the context of the error. Using two examples, 1) a forecasted value of 2000 and an observed value of 1500, as well as 2) a forecast of 10000 and an observation of 9500, both produce amount errors of 500. It is immediately noticeable that the second amount error is more desirable than the first even though the two are equal. In order to account for instances like this, the hourly measurements for "percent error" were tested—where *% error = (forecast – actual) ÷ actual * 100* –and a negative percent error represents an underforecast. Using a percent error, we can see that Example 1 was 33% greater than actual, and Example 2 was only 5.3% over the observed value. The average percent error (absolute value) before modification was 125%, and after modification, this shrank to 114%. The distribution of percent errors is also presented in Figure 17.

There are clear reductions in the number of underforecasts by the WRF-Chem, a small rise in more desirable errors (within 25% of true), but a marked increase in the number of overforecasts. This undesirable side-effect (overforecasting) is most likely caused by the diurnal function (*r(t)*) set in the "prep_chem_src" program in the WRF-Chem that artificially releases peak emission rates during dusk and sunrise "rush hour in cities" (Freitas et al. 2011). This leads to peak surface $PM_{2.5}$ overnight (trapped by a lowered boundary layer), and is visible in most of the days plotted in Figure 16. While peak values of observed $PM_{2.5}$ mass follow this trend, $PM_{2.5}$ *number* does not. Therefore, after bumping up the WRF-Chem run value sat 00Z (initialization) to match the observation, the artificial peak set by *r(t)* that follows shortly after 00Z overshoots the observed number concentration trend. If emission rates are manipulated in future work, they could be used to maximize the release of smaller particles during the times that number concentrations have been observed to peak.

Suggestions for Updated METAR

To introduce aerosol measurement into observational meteorology, a method that represents number concentrations as horizontal visibility estimates was demonstrated. These visibilities are suited for use in the METAR as a two-digit (imperial) or four-digit (metric) code. Using continuous data from 1 Apr to 13 Apr 2019, the author performed the LEEDR-visibility conversion on 46 sample number concentrations. This conversion requires the time-correspondent pressure, temperature and dewpoint. Thankfully, the array of weather sensors that took these measurements—to include a transmissometer

capable of testing our LEEDR-visibilities against for accuracy—was available during this time span within 25 meters of our CPC (CDE, 2019).

With the initial values gathered and plugged into the extinction construct detailed in Figure 11, 46 different values for total aerosol atmospheric extinction were calculated (Keefer, 2019). The results were then run through the conversion shown in Equation 3 to produce 46 horizontal visibilities. When compared to the transmissometer values observed at the same time (plotted in Figure 18), a linear regression produces a best-fit line with slope 0.62 (good, since slope=1.0 is a perfect 1:1 conversion) and a bias of +19.9 (positive y-intercept). This bias is artificially created because the transmissometer can only report visibility values up to 50-km, whereas LEEDR does not have this limitation. Nearly 70% of the time the transmissometer reported 50-km, the LEEDR-calculated visibility was greater than or equal to 50-km. The delayed prediction of a drop in visibility by LEEDR on 5 Apr and the early prediction on 7 Apr in Figure 18 remain unexplained.

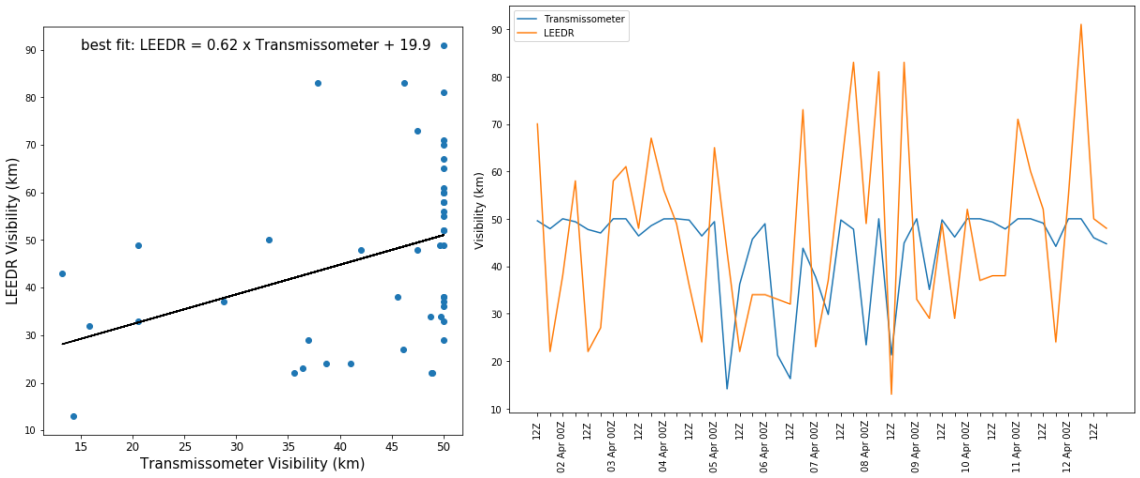

Figure 18. Linear regression between LEEDR and transmissometer visibilities (Left) Aerosol-based LEEDR predictions vs transmissometer-observed values (Right) (Center for Directed Energy, 2018)

The curve created in Figure 7—aerosol-related light extinction vs visibility—generally resembles an inverse relationship (where $visibility \propto 1/extinction$). In order to gain some insight as to how exactly each variable in the LEEDR process affected the end result, input parameters and the corresponding visibility result were compared (Figure 19). Since this calculation involved Mie theory, number-size distributions, refractive indices and ambient weather conditions, there was uncertainty regarding the correlation between $PM_{2.5}$ and the corresponding $\beta_{e,a}$ (and eventually visibility). This dependency turned out to be undeniable. The shape of the number concentration versus visibility distribution in Figure 20 shares the same trend of an inverse relationship. This means that $\beta_{e,a}$ is largely dependent on number concentration. The plots of pressure and humidity (dewpoint temperature divided by temperature) reveal very little correlation with the corresponding result on their own.

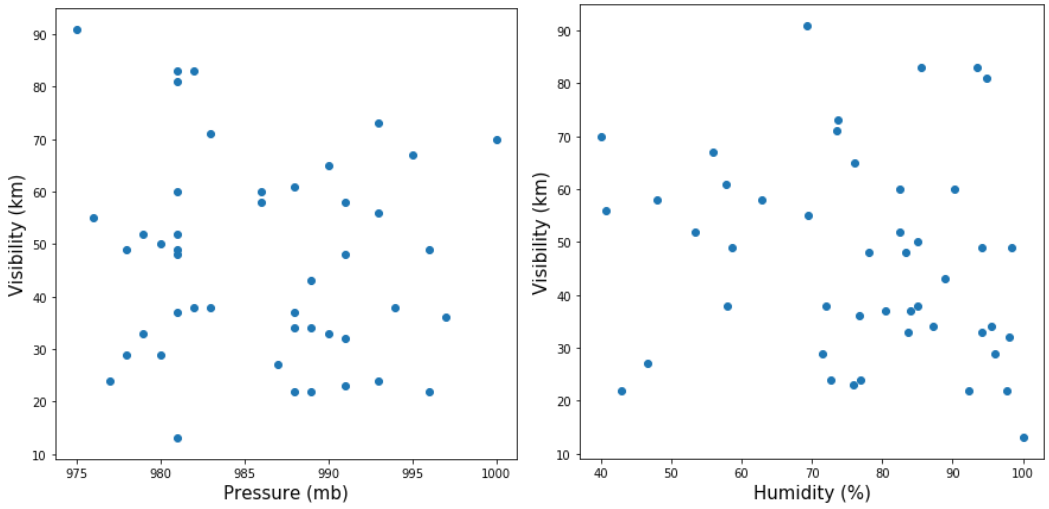

Figure 19. Observed pressure and corresponding visibilities (Left), humidity and visibility (Right)

Although similar in appearance to the $\beta_{e,a}$ curve in Figure 7, the shape of the number concentration scatter in Figure 20 is dispersed and not exactly a one-to-one function. This represents some fluctuations that arise under different weather conditions. By using colors in Figure 20 to identify pressure and humidity impacts on visibility, it becomes clear that humidity plays a more significant role in visibility restriction (hygroscopic growth of particles) than pressure. The lowest visibilities recorded had the highest humidity values. Since hydrometeor-related restrictions are included in our list of events that classify as not completely aerosol-based, a transmissometer remains the most accurate sensor to report visibility during these instances. A CPC-based visibility cutoff point of 95% humidity eliminates a great majority of outliers that deviate from a potential continuous function. This function is the key that serves to convert observed number concentration to a horizontal visibility estimate, and can be used at any location to encode $PM_{2.5}$ in the METAR.

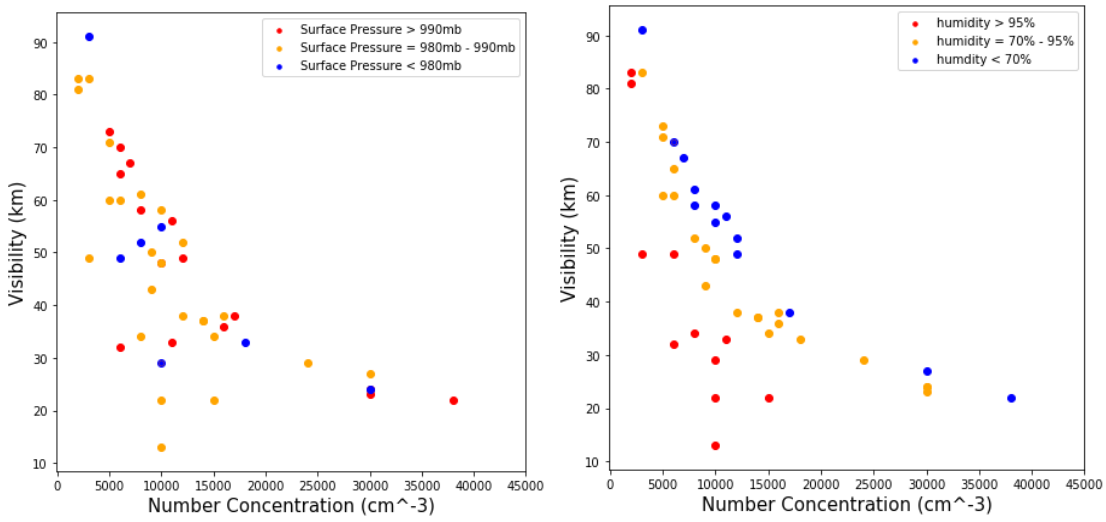

Figure 20. Number Concentrations and corresponding pressure observation (Left), outliers due to high humidities (Right)

After removing observations where the humidity was 95% or higher (reflected in Figure 21), two potential fit functions resembling the data using "polyfit" from Numpy were created (Rossum & Drake, 2010). Both fitted functions in Figure 21 are subject to change when more data is tested using LEEDR. An inverse function fit approaches infinity (different than the 250-km limit from Equation 3) as number concentration decreases to zero, and produces a minimum visibility of 24.4-km as number concentration increases to infinity. The polynomial has an upper limit of 99-km visibility at zero $PM_{2.5}$, but produces negative visibility values above number concentrations of 47,500-cm^{-3}. This visibility characterization limit extends when greater values of ambient $PM_{2.5}$ are added to the sample and fitted. Each observed point's distance (error) from the curve are represented as errorbars in Figure 22. Instead of using a root mean-square error, the curves' vertical (visibility) and horizontal (number concentration) errors are shown separately since the function is used with an observation.

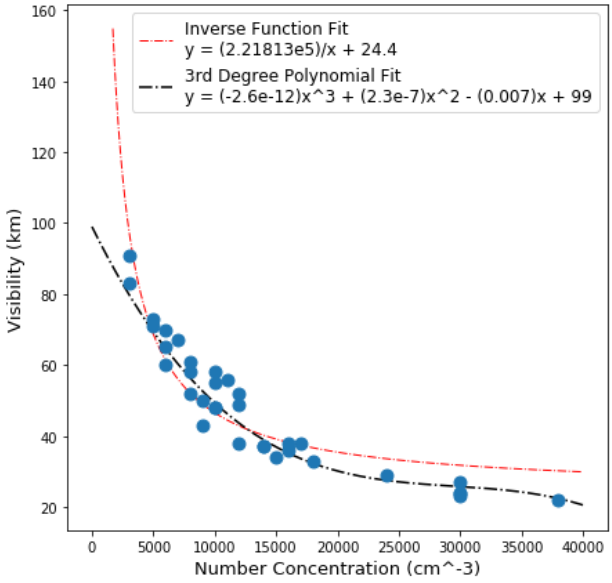

Figure 21. Two sample "conversion functions" for number concentrations with humidities less than 95%

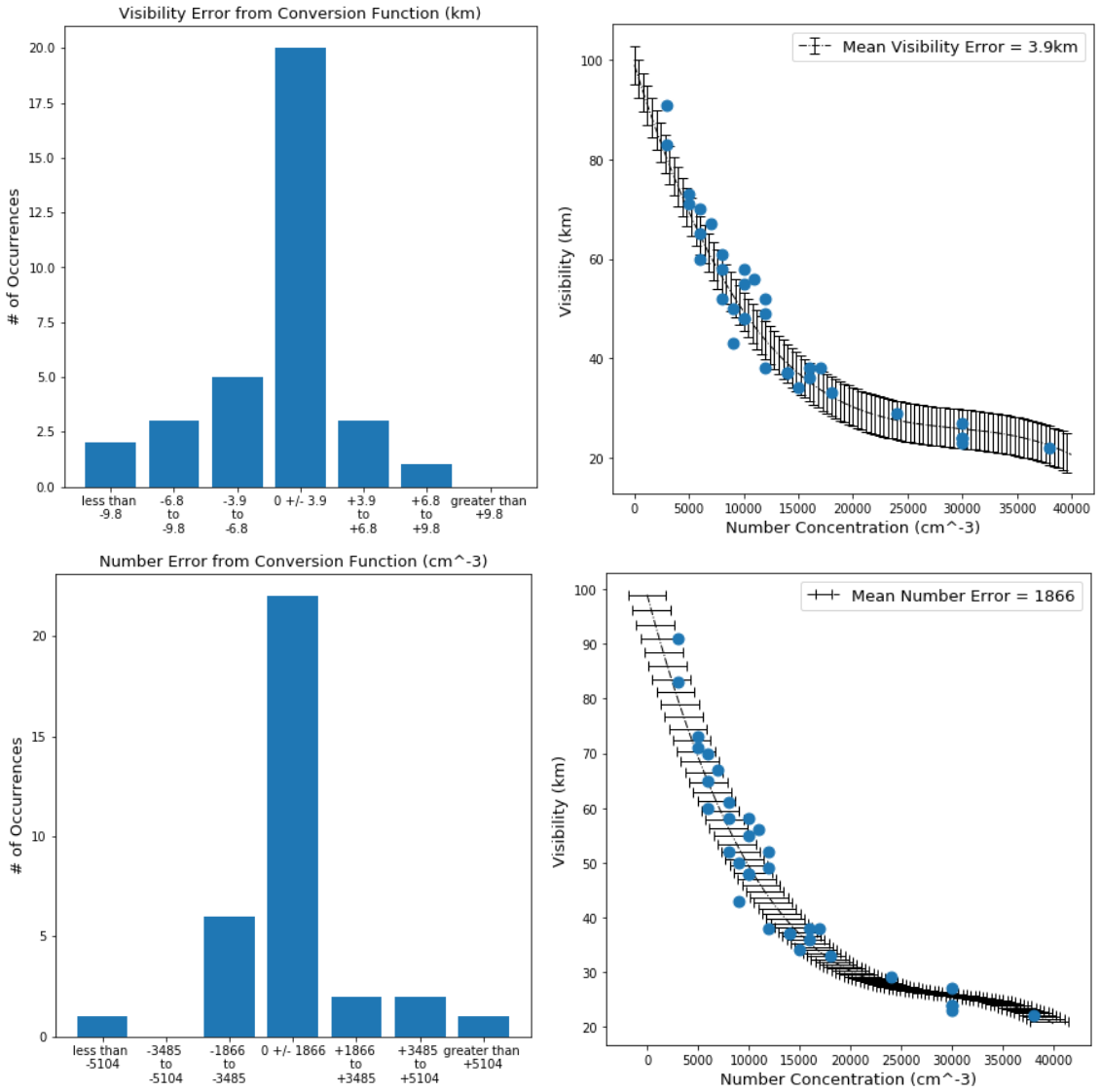

Figure 22. Equation 5 produces a visibility within 3.9km of the real visibility (Top); Equation 6 produces a number concentration within 1866 particles of observed (Bottom)

Since the polynomial function fit the data with smaller error than the simple inverse function, it is used as the basis for conversion. Higher-order polynomials become more useful as fitted functions when tested against larger sample sizes produced through LEEDR. The Converted Visibility function (Equation 5) is used to estimate horizontal visibility when given an observed number concentration. An interpreting meteorologist

that wants to extract the $PM_{2.5}$ number concentration from a METAR would use the inverse of Equation 5—a Converted Number Concentration function (Equation 6). While both polynomials are a little complex to write out, they are easily usable when run with some simple programming or a calculator.

$$Converted\ Visibility = [2.6e(-12)]\boldsymbol{n}^3 + [2.3e(-7)]\boldsymbol{n}^2 - [7e(-3)]\boldsymbol{n} + 99 \quad \text{(Equation 5)}$$

Where $\boldsymbol{n}$ = *$PM_{2.5}$ number concentration* (cm^{-3}) .

$$Converted\ Number\ Concentration = 0.02(V + 5.8e17)^{\frac{1}{3}} - (1.4e9)(V + 5.8e17)^{-\frac{1}{3}} + 3e4 \quad \text{(Equation 6)}$$

Where

$$V(\boldsymbol{v}) = \left[\sqrt{a\boldsymbol{v}^2 - b\boldsymbol{v} + c}\right] - d\boldsymbol{v} \ ,$$

a = 5.2e32 , b = 2.7e34 , c = 3.4e35 , d = 2.3e16 , and $\boldsymbol{v}$ = *horizontal visibility* (km).

Table 3. Observed $PM_{2.5}$ number concentration in increments of 2500 cm^{-3} and corresponding VIS observations rounded to the nearest ½ km or nearest SM.

Number Concentration (cm^{-3})	Visibility (nearest ½ km or SM)	METAR VIS (Metric)	METAR VIS (Imperial)
Not Available	Transmissometer	VVVV	VV SM
0	99.0 // 60	9990	60 SM
2,500	82.5 // 51	9825	51 SM
5,000	69.0 // 43	9690	43 SM
7,500	58.0 // 36	9580	36 SM
10,000	49.0 // 31	9490	31 SM
12,500	42.0 // 26	9420	26 SM
15,000	36.5 // 23	9365	23 SM
17,500	32.5 // 20	9325	20 SM
20,000	30.0 // 19	9300	19 SM
22,500	28.0 // 18	9280	18 SM
25,000	27.0 // 17	9270	17 SM
27,500	26.0 // 16	9260	16 SM
30,000	25.5 // 16	9255	16 SM
32,500	25.0 // 15	9250	15 SM
35,000	24.0 // 15	9240	15 SM
37,500	22.5 // 14	9225	14 SM
40,000	20.5 // 13	9205	13 SM
42,500	17.0 // 11	9170	11 SM
45,000	12.5 // 8	9125	8 SM
47,500	6.5 // 4	9065	4 SM
50,000+	Transmissometer	VVVV	VV SM

V. Conclusions and Recommendations

Overview

Although some of the key atmospheric influences (light extinction and cloud/precipitation formation) of $PM_{2.5}$ are described in this thesis, the question remains as to why its widespread observation is not maintained in observational meteorology. Organizations that currently gather aerosol data are not unified in their aims or their results. For example, the commercially-owned network PurpleAir gives the public access to real-time $PM_{2.5}$ observations via its website. However, its primary mission is to monitor air quality, and its sensors are designed to capture larger particles to represent aerosol mass. Number concentrations that include ultrafine particles as small as 10-nanometers are more relevant for meteorologists due to their roles as CCN and Rayleigh scatterers. If standardized, continuous observations were available, NWP models like the WRF-Chem would be able to initialize with real data instead of estimates based on climatic data. An additional and high-attention product that could include $PM_{2.5}$ information is the METAR. Since aerosol number concentrations are linked to light extinction, they could serve as the basis for a higher-fidelity VIS category.

Conclusions of Research

There is overall disagreement in practice within the aerosol measurement community. Some organizations, like the EPA and PurpleAir, focus on the monitoring of aerosol mass, while the WMO-led GAW prioritizes aerosol number. Mass measurements favor detection of large particles. $PM_{2.5}$ number concentrations are more useful and relevant for observational and numerical meteorology because they communicate the

abundance of particles in the accumulation and Aitken modes. There is no agreed-upon detection efficiency when using various sensors, and this can drastically impact the type and amount of particulate being captured in the reported value. Unless standardization occurs, NWP cannot reliably use aerosol data for initialization. Using a CPC, WRF-Chem $PM_{2.5}$ characterization errors for Dayton, OH were improved when initializing at a single point-location. This improvement can potentially be spread over an area if more points are initialized and interpolated. $PM_{2.5}$ observation can be integrated into the existing METAR framework as a converted horizontal visibility. This conversion can be performed by LEEDR or a polynomial function within acceptable error from that recorded by a transmissometer. The polynomial function can assume constant optical properties, size distributions, and meteorological conditions, making it a useful tool at any location to encode number concentration as a horizontal visibility estimate. The representation of $PM_{2.5}$ in the VIS category of the METAR would remain familiar for customers but become more descriptive for meteorologists.

Recommendations for Future Study

The aspect of this research that demands further attention is modification of the WRF-Chem. The method used to alter the model's input at the surface was entirely manual and is not suitable as a long-term solution that alters aerosol abundance throughout the entire vertical column. Data assimilation strategies that ingest data from several sources or locations would multiply the impacts that initialization has on the model's output. Initializing runs that begin at times other than 00Z could produce varying levels of improvement. It is advisable to test larger/smaller domains in different regions, during different times of the year, and for longer spans of time. It would be advantageous

to work alongside the GAW to petition the ICAO regarding standardization of $PM_{2.5}$ measurement, and a minimum detectable particle size when reporting number concentrations. Communication with the ICAO regarding improvement of the METAR and inclusion of aerosols as a local visibility would be beneficial going forward. Testing more data produced through LEEDR would aid in the creation of a more accurate conversion from number concentration to horizontal visibility. Comparing more converted visibilities to transmissometer values would also hone and advance this conversion process.

Summary

Ultimately, this thesis was intended to draw attention to the absence of aerosol observation in the meteorological community. The effects of $PM_{2.5}$ on horizontal visibility, cloud/precipitation formation, and atmospheric radiative transfer warrant its inclusion in observational meteorology. Just as NWP uses surface micro-meteorological observations to initialize each model run, atmospheric-chemistry models like the WRF-Chem can benefit from real-time surface aerosol measurements. Establishing a network of water-based CPCs to monitor $PM_{2.5}$ number concentrations down to 10-nm would provide the coverage necessary for models to interpolate values over an area. The sensors of this network could be incorporated within the arrays already located at ICAO weather stations. This would allow stations to routinely report $PM_{2.5}$ in METAR format as a comprehensive horizontal visibility. Interpreting meteorologists could then apply this knowledge to produce more informative and accurate forecasts for their clients.

Bibliography

AerosolInteractions.pdf. (2018). Retrieved December 21, 2019, from https://ruc.noaa.gov/wrf/wrf-chem/wrf_tutorial_2018/AerosolInteractions.pdf

Alfarra, Jimenez. (2004). Atmospheric Aerosols. Retrieved December 21, 2019, from http://cires1.colorado.edu/jimenez/Papers/Alfarra_PhD%20Thesis_1Chapter1_Introduction.pdf

Amaral, S. S., De Carvalho, J. A., Costa, M. A. M., & Pinheiro, C. (2015). An Overview of Particulate Matter Measurement Instruments. *Atmosphere*, *6*(9), 1327–1345. https://doi.org/10.3390/atmos6091327

Anthro_emission.pdf. (n.d.). Retrieved December 21, 2019, from https://ruc.noaa.gov/wrf/wrf-chem/wrf_tutorial_2018/Anthro_emission.pdf

Backman, J., Rizzo, L. V., Hakala, J., Nieminen, T., Manninen, H. E., Morais, F., Aalto, P. P., Siivola, E., Carbone, S., Hillamo, R., Artaxo, P., Virkkula, A., Petäjä, T., & Kulmala, M. (2012). On the diurnal cycle of urban aerosols, black carbon and the occurrence of new particle formation events in springtime São Paulo, Brazil. Atmospheric Chemistry and Physics, 12(23), 11733–11751. https://doi.org/10.5194/acp-12-11733-2012

Center for Directed Energy. (2018). *LEEDR User Guide*. Air Force Institute of Technology, Version 4.0.

Chin, M., Ginoux, P., Kinne, S., Torres, O., Holben, B. N., Duncan, B. N., Martin, R. V., Logan, J. A., Higurashi, A., & Nakajima, T. (2002). Tropospheric Aerosol Optical Thickness from the GOCART Model and Comparisons with Satellite and Sun Photometer Measurements. *Journal of the Atmospheric Sciences*, *59*(3), 461–483. https://doi.org/10.1175/1520-0469(2002)059<0461:TAOTFT>2.0.CO;2

Diehl, T., Crippa, M., Guizzardi, D., Janssens-Maenhout, G., Dentener, F., Koffi, B., Solazzo, E., Galmarini, S., European Commission, & Joint Research Centre. (2016). *Hemispheric Transport of Air Pollution (HTAP) specification of the HTAP2 experiments: Ensuring harmonized modelling.* Publications Office.

Dr. Mian Chin. (n.d.). Retrieved December 21, 2019, from https://acd-ext.gsfc.nasa.gov/People/Chin/gocartinfo.html

Emission_guide.pdf. (n.d.). Retrieved December 21, 2019, from https://ruc.noaa.gov/wrf/wrf-chem/Emission_guide.pdf

Fiorino, S. T., Bartell, R. J., Krizo, M. J., Caylor, G. L., Moore, K. P., Harris, T. R., & Cusumano, S. J. (2008). *A first principles atmospheric propagation & characterization tool: The laser environmental effects definition and reference (LEEDR)* (O. Korotkova, Ed.; p. 68780B). https://doi.org/10.1117/12.763812

Fiorino, S. T., Randall, R. M., Via, M. F., & Burley, J. L. (2014). Validation of a UV-to-RF High-Spectral-Resolution Atmospheric Boundary Layer Characterization Tool. *Journal of Applied Meteorology and Climatology*, *53*(1), 136–156. https://doi.org/10.1175/JAMC-D-13-036.1

Fiorino, S.T., Peckham, S. E., Schmidt, J. E., Keefer, K. J. (2019) Evaluation of Aerosol Characterizations within the WRF-Chem GOCART Scheme. Unpublished manuscript.

Freitas, S. R., Longo, K. M., Alonso, M. A., Pirre, M., Marecal, V., Grell, G., ... & Gácita, M. S. (2011). PREP-CHEM-SRC-1.0: a preprocessor of trace gas and aerosol emission fields for regional and global atmospheric chemistry models. *Geoscientific Model Development*, *4*(2), 419.

Global Atmosphere Watch Programme (GAW) | World Meteorological Organization. (n.d.). Retrieved January 5, 2020, from https://community.wmo.int/activity-areas/gaw

GETTING STARTED: EMISSIONS INVENTORY METHODS FOR PM-2.5. (1999). Retrieved December 21, 2019, from https://www.epa.gov/sites/production/files/2015-08/documents/ix01.pdf

Grell, G. A., Peckham, S. E., Schmitz, R., McKeen, S. A., Frost, G., Skamarock, W. C., & Eder, B. (2005). Fully coupled "online" chemistry within the WRF model. *Atmospheric Environment*, *39*(37), 6957–6975. https://doi.org/10.1016/j.atmosenv.2005.04.027

Hinds, W. C. (1999). *Aerosol technology: Properties, behavior, and measurement of airborne particles* (2nd ed). Wiley.

Hunter, J.D. (2007). *Matplotlib: A 2D Graphics Environment*. *Computing in Science & Engineering*, vol. 9, no. 3, pp. 90-95.

Janssens-Maenhout, G., Dentener, F., Van Aardenne, J., Monni, S., Pagliari, V., Orlandini, L., Klimont, Z., Kurokawa, J., Akimoto, H., Ohara, T., Wankmüller, R., Battye, B., Grano, D., Zuber, A., Keating, T., European Commission, Joint Research Centre, & Institute for Environment and Sustainability. (2012). *EDGAR-HTAP: A harmonized gridded air pollution emission dataset based on national inventories.* Publications Office. http://dx.publications.europa.eu/10.2788/14102

Janssens-Maenhout, G., Crippa, M., Guizzardi, D., Dentener, F., Muntean, M., Pouliot, G., Keating, T., Zhang, Q., Kurokawa, J., Wankmüller, R., Denier van der Gon, H., Kuenen, J. J. P., Klimont, Z., Frost, G., Darras, S., Koffi, B., & Li, M. (2015). HTAP_v2.2: A mosaic of regional and global emission grid maps for 2008 and 2010 to study hemispheric transport of air pollution. Atmospheric Chemistry and Physics, 15(19), 11411–11432. https://doi.org/10.5194/acp-15-11411-2015

Kahn, R. A., Berkoff, T. A., Brock, C., Chen, G., Ferrare, R. A., Ghan, S., Hansico, T. F., Hegg, D. A., Martins, J. V., McNaughton, C. S., Murphy, D. M., Ogren, J. A., Penner, J. E., Pilewskie, P., Seinfeld, J. H., & Worsnop, D. R. (2017). SAM-CAAM: A Concept for Acquiring Systematic Aircraft Measurements to Characterize Aerosol Air Masses.

Bulletin of the American Meteorological Society, 98(No 10), 2215–2228. https://doi.org/10.1175/BAMS-D-16-0003.1

Kazil, J. (2009). Introduction to aerosol modeling with WRF/Chem. 30.

Koshmeider, H. (1926), Theorie der horizontale Sichtweite, B*eitr. Atmos. Phys.*, 12, 33 – 55.

Liou, K.-N. (2002). *An introduction to atmospheric radiation* (2nd ed). Academic Press.

Lynch, P. (2006). The origins of computer weather prediction and climate modeling. *Journal of Computational Physics*, *227*(7), 3431–3444. https://doi.org/10.1016/j.jcp.2007.02.034

Malm, W., & Service, N. P. (n.d.). *Introduction to Visibility*. 79.

Masri, S., Garshick, E., Hart, J., Bouhamra, W., & Koutrakis, P. (2017). Use of Visual Range Measurements to Predict PM2.5 Exposures in Southwest Asia and Afghanistan. *Journal of the Air & Waste Management Association (1995)*, *67*(1), 75–85. https://doi.org/10.1080/10962247.2016.1243169

NOAA's National Weather Service-Aviation Weather Center Homepage. (n.d.). *AWC - Aviation Weather Center*. Retrieved January 5, 2020, from https://www.aviationweather.gov/metar

Pagowski, M., Liu, Z., Grell, G. A., Hu, M., Lin, H.-C., & Schwartz, C. S. (2014). Implementation of aerosol assimilation in Gridpoint Statistical Interpolation (v. 3.2) and WRF-Chem (v. 3.4.1). *Geoscientific Model Development*, *7*(4), 1621–1627. https://doi.org/10.5194/gmd-7-1621-2014

Pagowski, M., Grell, G. A., McKeen, S. A., Peckham, S. E., & Devenyi, D. (2010). Three-dimensional variational data assimilation of ozone and fine particulate matter observations: Some results using the Weather Research and Forecasting—Chemistry model and Grid-point Statistical Interpolation. Quarterly Journal of the Royal Meteorological Society, 136(653), 2013–2024. https://doi.org/10.1002/qj.700

Peckham, S., G. A. Grell, S. A. McKeen, M. Barth, G. Pfister, C. Wiedinmyer, J. D. Fast, W. I. Gustafson, R. Zaveri, R. C. Easter, J. Barnard, E. Chapman, M. Hewson, R. Schmitz, M. Salzmann, S. Freitas. *WRF-Chem version 3.8.1 user's guide.* https://doi.org/10.7289/V5/TM-OAR-GSD-48

Petty, G. W. (2006). *A first course in atmospheric radiation* (2nd ed). Sundog Pub.

Rogers, R. R., & Yau, M. K. (1996). *A short course in cloud physics* (3. ed., reprint). Butterwoth-Heinemann.

Rossum, G. van & Drake, F. L. (2010). *The Python language reference* (Release 3.0.1 [Repr.]). Python Software Foundation.

US EPA. (1998). *Guidance for Using Continuous Monitors in $PM_{2.5}$ Monitoring Networks.* Retrieved December 21, 2019, from https://www3.epa.gov/ttnamti1/files/ambient/pm25/r-98-012.pdf

U.S. Air Force Research Laboratory—DoD Supercomputing Resource Center. (n.d.). Retrieved January 5, 2020, from https://www.afrl.hpc.mil/index.html

U.S. Air Force Research Laboratory—DoD Supercomputing Resource Center—SGI Ice X (Thunder) User Guide. (n.d.). Retrieved December 21, 2019, from https://www.afrl.hpc.mil/docs/thunderUserGuide.html

US EPA, O. (2015, February 6). *EPA's Report on the Environment (ROE)* [Reports and Assessments]. US EPA. https://www.epa.gov/report-environment

US EPA, O. (2016, August 11). *Evaluation of Emerging Air Pollution Sensor Performance* [Overviews and Factsheets]. US EPA. https://www.epa.gov/air-sensor-toolbox/evaluation-emerging-air-pollution-sensor-performance

Weather Forecasting and Research. (2017). *ARW Users Guide V3.8*. Retrieved December 21, 2019, from https://www2.mmm.ucar.edu/wrf/users/docs/user_guide_V3.8/ARWUsersGuideV3.8.pdf

Werner, M., Kryza, M., Pagowski, M., & Guzikowski, J. (2019). Assimilation of PM2.5 ground base observations to two chemical schemes in WRF-Chem – The results for the winter and summer period. *Atmospheric Environment, 200*, 178–189. https://doi.org/10.1016/j.atmosenv.2018.12.016

World Meteorological Organization. (2008). *Guide to meteorological instruments and methods of observation*. WMO.

World Meteorological Organization & Global Atmosphere Watch. (2016). *WMO/GAW aerosol measurement procedures: Guidelines and recommendations.*

Zhao, T. L., Gong, S. L., Huang, P., & Lavoué, D. (2012). Hemispheric transport and influence of meteorology on global aerosol climatology. *Atmospheric Chemistry and Physics Discussions, 12*(4), 10181–10221. https://doi.org/10.5194/acpd-12-10181-2012